Global Biogeochemical Cycles

RESEARCH ARTICLE
10.1029/2018GB005939

Projected Centennial Oxygen Trends and Their Attribution to Distinct Ocean Climate Forcings

Yohei Takano[1,2], **Takamitsu Ito**[1], **and Curtis Deutsch**[3]

[1]School of Earth and Atmospheric Sciences, Georgia Institute of Technology, Atlanta, GA, USA, [2]Max-Planck Institute for Meteorology, Hamburg, Germany, [3]School of Oceanography, University of Washington, Seattle, WA, USA

Key Points:
- We performed sensitivity experiments to quantify the impacts of different surface climatic forcing on the centennial oxygen trends
- Decrease of AOU in the tropical oceans are caused predominantly by ocean warming, with small effects from hydrological and wind forcing
- Changes in ocean circulation and biological oxygen consumption almost equally contribute to the long-term decrease in tropical Pacific AOU

Correspondence to:
Y. Takano,
yohei.takano@mpimet.mpg.de

Citation:
Takano, Y., Ito, T., & Deutsch, C. (2018). Projected centennial oxygen trends and their attribution to distinct ocean climate forcings. *Global Biogeochemical Cycles*, *32*, 1329–1349. https://doi.org/10.1029/2018GB005939

Received 10 APR 2018
Accepted 17 AUG 2018
Accepted article online 23 AUG 2018
Published online 13 SEP 2018

Abstract We explore centennial changes in tropical Pacific oxygen (O_2) using numerical models to illustrate the dominant patterns and mechanisms under centennial climate change. Future projections from state-of-the-art Earth System Models exhibit significant model to model differences, but decreased solubility and weakened ventilation together deplete thermocline O_2 in middle to high latitudes. In contrast, the tropical thermocline O_2 undergoes much smaller changes or even a slight increase. A suite of sensitivity experiments using a coarse resolution ocean circulation and biogeochemistry model show that ocean warming is the leading cause of global deoxygenation in the thermocline across all latitudes with secondary contributions from changes in hydrological cycles and wind stress modulating regional changes in O_2. The small O_2 changes in the tropical Pacific thermocline reflect near-complete compensation between the solubility decrease due to warming and reduction in apparent oxygen utilization (AOU). We further quantified the changes in AOU due to contributions from changes in water mass age and biological remineralization from the sensitivity experiments. The two effects almost equally contribute to the reduction of AOU in the tropical Pacific thermocline (43% for physical circulations and 57% for biology). Our results suggest that better understanding of water mass changes in the tropical oceans is key to improving projections and reducing the uncertainties of future O_2 changes.

Plain Language Summary Global warming in the next hundred years could lead to a large amount of oxygen loss from the ocean. This could impact not only the marine ecosystem but also fisheries. We use model simulations to investigate how long-term climate change, such as changes in sea surface temperature, precipitation, and winds, under the anthropogenic transient could impact oceanic oxygen loss in the next hundred years. The ocean loses oxygen in most of the regions but tropical oceans could actually gain oxygen regionally. We investigate what causes these unique oxygen changes in the tropical Pacific Ocean. The counterintuitive oxygen changes in the tropical Pacific Ocean are likely due to, by an almost equal amount of effects, changes in water mass supply due to changes in circulations and changes in biological activity, that is, consumption of oxygen through respiration. Tropical oceans are sensitive to oxygen loss because of its impact on marine ecosystems. Our study could provide a better understanding of future oxygen loss in the ocean.

1. Introduction

Dissolved oxygen (hereafter O_2) is a major driver of marine ecosystems and biogeochemistry with far-reaching influence on physiology (Seibel, 2010; Vaquer-Sunyer & Duarte, 2008), species distributions (Deutsch et al., 2015), and the nitrogen cycle (Codispoti, 1995; Codispoti et al., 2001; Voss et al., 2013). Previous studies indicate that global warming could reduce the amount of O_2 on the global scale (Bopp et al., 2013; Cocco et al., 2013; Keeling & Garcia, 2002; Matear & Hirst, 2003). A decline of oceanic O_2 under global warming is considered a major threat to the marine ecosystem along with ocean warming and acidification (Gruber, 2011). In a warming ocean, the solubility of gases decreases. Vertical exchange of water masses and overturning circulations may also weaken as the density stratification of the upper ocean increases due to the combined effects of ocean warming and increased precipitation at high latitudes (Capotondi et al., 2012). These changes will reinforce the solubility-driven O_2 loss by weakening the circulation supply of O_2 to waters below the mixed-layer (e.g., Keeling et al., 2010).

Since global warming and associated climate change proceed gradually on the centennial timescale, its impact on ocean biogeochemical tracers may be obscured by energetic interannual and decadal variability (Long et al., 2016; Lovenduski et al., 2016; McKinley et al., 2016, 2017). The spatial and temporal coverage

Table 1
List of the Subset of the Coupled Model Intercomparison Project Phase 5 ESMs Used in This Study Including Modeling Groups, Institute ID, Model Names, and References

Modeling group/center	Institute ID	Model name
NOAA Geophysical Fluid Dynamics Laboratory (Dunne et al., 2012)	NOAA GFDL	GFDL ESM 2M GFDL ESM 2G
Institut Pierre-Simon Laplace (Dufresne et al., 2013)	IPSL	IPSL CM5A MR
Met Office Hadley Centre (additional HadGEM2-ES realizations contributed by Instituto Nacional de Pesquisas Espaciais; W. J. Collins et al., 2011)	MOHC (additional realization by INPE)	HadGEM2-ES
Max-Planck-Institut für Meteorologie (Max-Planck Institute for Meteorology; Giorgetta et al., 2013)	MPI-M	MPI-ESM-MR
Community Earth System Model Contributors (Moore et al., 2013)	NSF-DOE-NCAR	CESM1 (BGC)

Note. ESM = Earth System Model.

of historic observations are sparse and irregular, which fundamentally limit our understanding of anthropogenic transients of ocean biogeochemical tracers (Lovenduski et al., 2015; McKinley et al., 2016, 2017). Therefore, numerical models have been the primary tool to investigate the centennial-scale, anthropogenic ocean deoxygenation. Simulations based on state-of-the-art Earth System Models (ESMs) predict a global deoxygenation under a warming climate but there are large model-to-model differences in regional projections, especially Oxygen Minimum Zones (OMZs) in the tropical oceans (Bopp et al., 2013; Cabré et al., 2015; Cocco et al., 2013; Shigemitsu et al., 2017). These ESMs are highly complex, and different model responses are often difficult to interpret due to numerous differences in model architecture, configurations, and parameter choices even though the greenhouse gas forcing is applied in a consistent way.

The objective of this study is to better understand the mechanisms behind the centennial-scale responses of oceanic O_2 to anthropogenic climate change in the future. We focus on understanding the future projections of oceanic O_2 over a centennial timescale, not on the historical changes in oceanic O_2. The observational studies indicate significant decrease in global and tropical O_2 (Helm et al., 2011; Ito et al., 2017; Stramma et al., 2008; Schmidtko et al., 2017) but these decadal changes in O_2 could also be associated with modes of natural climate variability such as the Pacific Decadal Oscillation (Czeschel et al., 2012; Deutsch et al., 2011; Ito & Deutsch, 2013). The ESMs do not necessarily reproduce the specific phases of internal variability matching the observations, which may have played crucial roles in setting the trajectory of O_2 changes during the historical period. These topics are not the focus of this study. We particularly focus on studying future projections of O_2 in the tropical Pacific Ocean because it contains the largest volume of low O_2 water in the global ocean and its future response to climate change highly varies across models. We examine the effect of centennial climate forcing as transient changes to surface buoyancy and momentum fluxes of the oceans, including ocean warming, changes in the hydrological cycle, and surface atmospheric wind stress. This study takes a hierarchical approach using models of different complexities to reveal robust aspects of model behavior and thus achieve a deeper level of understanding. Simpler models can be manipulated to perform illustrative sensitivity experiments, which can help interpret the behavior of complex ESMs. It is not yet clear how each aspect of atmospheric and oceanic processes impacts the evolution of oceanic O_2. Our aim is to examine the effects of distinct climatic forcing through a suite of sensitivity experiments using a simpler ocean circulation and biogeochemistry model.

The structure of this paper is as follows. We describe the model setup and experimental design in section 2. In section 3, we present the validation and overview of the simulated climatological and centennial changes in O_2. We show our results from sensitivity experiments and ESMs interpreting the centennial O_2 changes in section 4. We will summarize our study and discuss implications in section 5.

2. Data and Methods

2.1. State-Of-The-Art ESM Projections

We analyze the outputs from a subset of ESM simulations performed as a part of Coupled Model Intercomparison Project Phase 5 (CMIP5; see Table 1). Historical climate reconstructions based on past

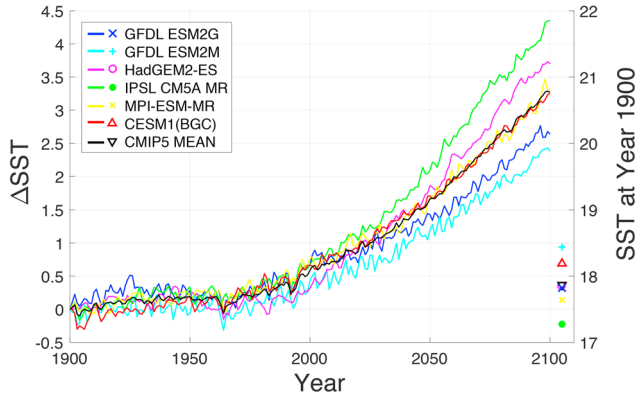

Figure 1. Time series of global mean SST anomalies from the selected CMIP5 models (shown in Table 1). SST anomalies are the differences from the values in 1900 (shown as colored shape on the right of the figure). We used CMIP5 (multimodel) mean SST anomaly (CMIP5 MEAN, black line) to conduct sensitivity experiments (see section 3.2 for details). SST = sea surface temperature; ESM = Earth System Model; CMIP5 = Coupled Model Intercomparison Project Phase 5.

estimated radiative forcing are merged with a future climate scenario under a radiative forcing of approximately 8.5 W/m^2 at the end of the century (RCP8.5; Meinshausen et al., 2011; Taylor et al., 2012). The ESMs represent marine ecosystems and biogeochemical cycles including O_2, CO_2, and nutrients with diverse parameterization of biological production, export, and remineralization of organic matter in the water column. We analyzed annual-mean model output after interpolating onto a 1° × 1° longitude-latitude grid at 33 vertical z-levels consistent with the World Ocean Atlas 2009 (WOA2009; Garcia et al., 2010).

2.2. Centennial Climate Change in the CMIP5 Projections

Centennial trends in surface climate could significantly influence ocean circulation and associated biogeochemical cycles. Common features in centennial-scale surface climate change projected in ESM simulations (M. R. Collins et al., 2013) are (1) increase in sea surface temperature (M. R. Collins et al., 2013; Thomas et al., 2013; Vallis et al., 2015), (2) acceleration of the hydrological cycles (Held & Soden, 2006; Schneider et al., 2010), (3) a trend toward a stronger and poleward shifted southern hemisphere jet (Gillett & Fyfe, 2013; G. J. Marshall, 2003; Thompson et al., 2000), and (4) a possible weakening of the Walker circulation and associated Pacific trade winds (Tokinaga et al., 2012; Vecchi et al., 2006). As a reference for the increase in sea surface temperature, we calculated centennial changes in global mean sea surface temperature from the output of CMIP5 historical and RCP8.5 future simulations (1900–2100). The increase in sea surface temperature starts to accelerate around 2000 reaching 2.5–4.5 °C of global mean warming by 2100 relative to 1900 (Figure 1).

Long-term climate changes are also evident in both zonal mean freshwater flux (i.e., evaporation minus precipitation, E − P) and the Southern Hemisphere zonal wind stress from CMIP5 projections toward 2100 (Figures 2a and 2b; e.g., Swart et al., 2015). Zonal wind stress also shows gradual weakening of the trade winds (~5 × 10^{-3} N/m^2, positive eastward) in the eastern tropical Pacific region (Figure 2c). Zonal wind stress in future projections also exhibits strong positive anomalies in the off-equatorial Pacific region at around 15°N (Figure 2c). These changes in equatorial wind stress could impact ocean gyre circulations and primary production through changes in nutrient supply in this region.

Based on the analysis of surface atmospheric fields from the CMIP5 RCP8.5 projections (Figures 1 and 2), we designed sensitivity experiments mimicking these centennial-scale climate changes. Despite the uncertainties and complicated spatial patterns of the simulated surface climate change, we kept our climate forcing as simple as possible including the essence of all processes (1–4) and the main features of future climate change from CMIP5 RCP8.5 projections. This will simplify our interpretation of the results from sensitivity experiments.

2.3. The Ocean Model for Sensitivity Experiments

It is difficult to quantify the relative importance of different climatic forcing from analyzing the outputs from ESMs with limited diagnostic information. Thus, we conduct a suite of sensitivity experiments using a coarse-resolution ocean circulation and biogeochemistry model. The model is essentially identical to the model used by Ito et al. (2015). The model is based on the Massachusetts Institute of Technology general circulation model (MITgcm; J. Marshall, Adcroft, et al., 1997; J. Marshall, Hill, et al., 1997) with a simple biogeochemistry component (Dutkiewicz et al., 2005; Parekh et al., 2005). The model has a semiglobal bathymetry in a 2.8° × 2.8° longitude-latitude grid, and 23 nonuniform vertical z-levels with increased resolution near the surface. The Arctic Ocean is not included in this model. Mesoscale eddies are parameterized using the isopycnal thickness diffusion scheme (Gent & McWilliams, 1990) with a uniform constant isopycnal thickness diffusivity of 1,000 m^2/s, and tracers are also subject to along-isopycnal diffusion at the same rate (Redi, 1982). Vertical tracer diffusion is parameterized using the Bryan and Lewis (1979) scheme, in which vertical diffusivity is set to 0.3 × 10^{-4} m^2/s in the upper 2,000 m and increases to 1 × 10^{-4} m^2/s in the interior ocean following an arctangent profile. The mixed-layer processes are parameterized using the K-Profile Parameterization

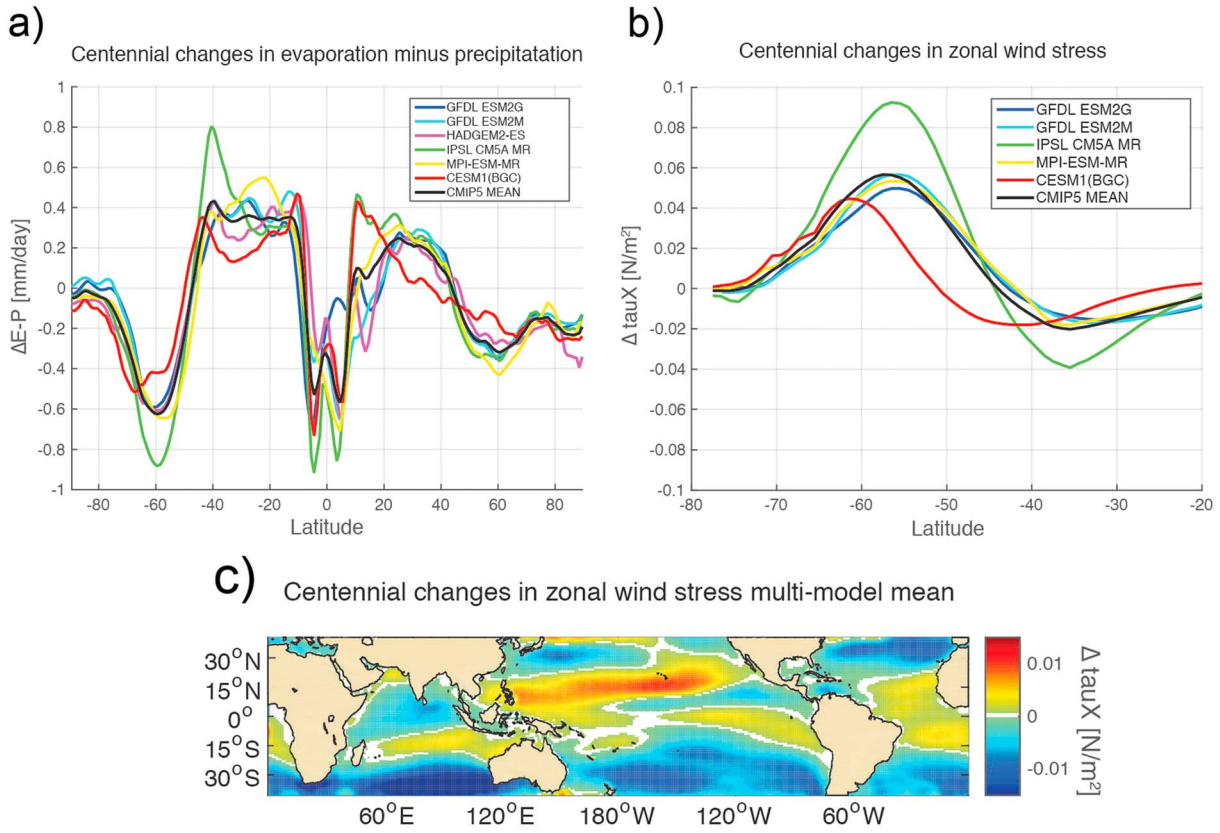

Figure 2. Centennial changes (i.e., RCP8.5 mean, 2070–2100, minus preindustrial mean, 1900–1930) in zonal mean (a) evaporation minus precipitation (E − P; mm/day) and (b) zonal wind stress (N/m^2) in the Southern hemisphere. (c) Centennial changes in tropical zonal wind stress (N/m^2) based on the multimodel mean data from the CMIP5 models. E – P = evaporation minus precipitation; ESM = Earth System Model; CMIP5 = Coupled Model Intercomparison Project Phase 5.

scheme (Large et al., 1994). The model carries dissolved phosphate, dissolved organic phosphorus, O_2, and dissolved iron. In addition, the model carries an ideal age tracer, which approximates the timescale over which respiration depletes O_2 in water parcels that have left the surface ocean.

We spin up the model with climatological wind stress, freshwater flux, and heat flux fields (Jiang et al., 1999; Trenberth et al., 1989). To maintain surface temperature-salinity properties close to the observations, we also applied Newtonian relaxation to the sea surface temperature and salinity toward monthly climatology (Levitus et al., 1994; Levitus & Boyer, 1994) with timescales of 60 and 90 days, respectively. Because of the lack of sea-ice/ice-shelf processes and highly smoothed topography, the model cannot adequately form Antarctic Bottom Water. To address this issue, we locally raised the climatological salinity in the polar Southern Ocean for the restoring boundary condition to increase deep ventilation in the southern high latitudes. This modification of salinity restoring accelerated the lower overturning circulation and increased the O_2 concentration of the abyssal Southern Ocean in much better agreement with observations.

After spinning up the model for several millennia to achieve a steady state, we performed sensitivity experiments.

2.4. Experimental Design

Based on previous studies (see section 2.2) and projected climate change in the CMIP5 simulations, we perform idealized sensitivity experiments including the following forcing.

A *MITgcm-Warm*: A globally uniform increase in the sea surface temperature (Figure 1).
B *MITgcm-EmP*: Intensification of freshwater flux (E − P) by 10% per century (Figure 3a).
C *MITgcm-SAM*: Intensification and poleward shift of the zonal and meridional wind stress over the Southern Ocean (Figure 3b).

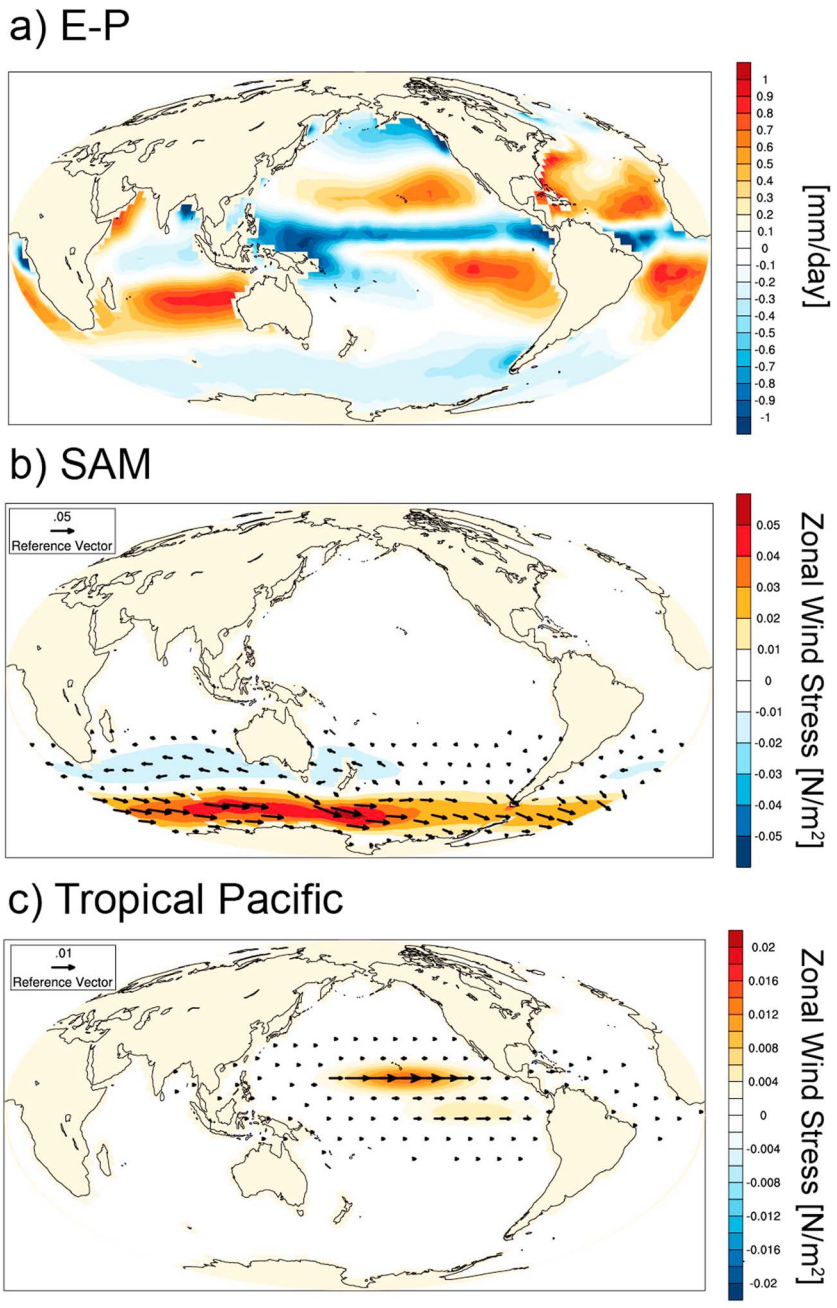

Figure 3. Spatial patterns of (a) centennial changes (after 200 years) in E − P and (b) and (c) wind stresses used for perturbation experiments (vectors, with zonal wind stress magnitudes in shading). Zonal and meridional wind stresses in (b) are from the SAM-regression based wind stresses. (c) Idealized representation of tropical Pacific wind stress changes expressed as Gaussian bump anomalies. E – P = evaporation minus precipitation; SAM = Southern Annular Mode. This figure has been drawn by the NCL (The NCAR Command Language (Version 6.3.0), 2016).

D *MITgcm-Trade*: Changes in the zonal wind stress over the equatorial Pacific and the off-equatorial Pacific regions (Figure 3c).

E *MITgcm-ALL*: Inclusion of all forcing patterns (A–D; ALL).

The warming experiment (A) is implemented by nudging the sea surface temperature with a trend superimposed over the mean seasonal cycle. The rate of temperature increase is based on the ensemble mean of the CMIP5 models (Figure 1, black line). The freshwater experiment (B) is implemented by globally modulating the amplitude of monthly evaporation minus the precipitation field while maintaining the same spatial

pattern as the climatology (Figure 3a). The rate of increase is set to 10% per century as a simple analog for the intensification of the hydrological cycle. We implement a trend in the Southern Ocean wind stress (C) by adding wind stress anomalies (centennial trend) between 21 and 88.6°S. The wind stress anomalies for (C) are based on regression coefficients between the normalized monthly Southern Annular Mode (SAM) index (G. J. Marshall, 2003) and National Centers for Environmental Prediction and National Center for Atmospheric Research reanalysis monthly mean zonal and meridional wind stress (Kalnay et al., 1996) from 1957 to 2015 for each month. The SAM is characterized by the intensification of winds and the shift of jet position between middle to high latitudes (e.g., Thompson et al., 2000). Thus, the wind stress regression fields based on SAM capture the essential characteristics of changes in the Southern Ocean jet (Solomon & Polvani, 2016; Swart et al., 2015). The magnitudes of these changes in surface buoyancy and momentum fluxes are roughly equivalent to the multimodel mean changes in the CMIP5 RCP8.5 projection. Finally, we impose positive anomalies of zonal wind stress as Gaussian anomalies in the eastern equatorial Pacific Ocean and off-equatorial Pacific Ocean. This forcing is based on the centennial trend in the wind stress of CMIP5 models (Figure 3c) and is meant to be an idealized representation of the weakened equatorial Pacific trade wind (Tokinaga et al., 2012; Vecchi et al., 2006). These changes in the tropical wind stress have been associated with global warming (Ma & Xie, 2013; Xie et al., 2010). The Gaussian patches are centered over the equator in the eastern tropical Pacific Ocean and off-equatorial Pacific Ocean at around 15°N. The magnitudes are set to 3×10^{-5} N·m^{-2}·year^{-1} in the eastern tropical Pacific Ocean and 1.5×10^{-4} N·m^{-2}·year^{-1} for the off-equatorial Pacific Ocean (Figure 3c). We also perform a control run (*MITgcm-CTL*) without any perturbation. Comparing results from each sensitivity experiment with the control run enables us to evaluate the response to each idealized climate forcing.

3. Multimodel Projections of Thermocline Deoxygenation

3.1. Model Validation Based on Climatology

We first overview the climatological mean O_2 distributions between CMIP5 model outputs, MITgcm-CTL, and WOA2009 (Garcia et al., 2010). Here we focus on analyzing the O_2 at 400 m (435 m for MITgcm-CTL) as a metric of the main thermocline O_2. This depth is in the core of the O_2 minimum layer in the tropical oceans, typically located within $26.0 < \sigma_\theta < 27.0$ and 200 m $<$ z $<$ 700 m (Karstensen et al., 2008; Stramma et al., 2008). The CMIP5 climatology is based on the 30-year mean of the late twentieth century (1971–2000). The CMIP5 models and MITgcm-CTL can generally reproduce the large-scale climatological distributions of thermocline O_2 in WOA2009 (Figure 4). The models capture the overall zonal mean structures of O_2 including the O_2 minimum zones in the tropics and subarctic North Pacific, and the well ventilated O_2-rich water mass in the Southern Ocean. However, the O_2-rich water mass in each model does not penetrate as much into the interior ocean as we see in WOA2009 in the Southern Hemisphere (Figures 4d–4f). The Antarctic Intermediate Water mass formation in the models could be underestimated in both CMIP5 models and MITgcm-CTL. The location of tropical OMZs (i.e., vertical oxycline in the tropics) is also deeper in MITgcm-CTL compared to the CMIP5 models and observations. This could be a result of higher background vertical diffusivity in MITgcm compared to that of CMIP5 models.

A comprehensive analysis of simulated tropical Pacific OMZs in the CMIP5 models is presented in Cabré et al. (2015) with detailed examination of the horizontal and vertical structure and volumes of OMZs. Here we briefly summarize the model mean bias, spatial correlation of O_2 at 400 m (435 m for MITgcm-CTL), and hypoxic volume simulated in the models. Globally, the mean bias among models ranges from −30.94 to +13.63 mmol/m^3. When the domain is limited to the Pacific basin (north of 20°S) the mean bias takes an even wider range from −42.96 to +30.98 mmol/m^3. The spatial pattern is overall well reproduced; the spatial correlation coefficient (R) is within a relatively high range from 0.87 to 0.96 in the global domain (see Table 2 for details), and it slightly decreases over the Pacific domain (range from 0.76 to 0.93) for CMIP5 models. The MITgcm-CTL exhibits reasonable mean O_2 level as well as spatial pattern comparable to CMIP5 models. The global mean bias is −17.79 mmol/m^3 and its global spatial correlation coefficient is 0.90. It overestimates the mean oxygen level in the Pacific basin with a mean bias of +21.3 mmol/m^3, while the spatial correlation coefficient decreases (R = 0.85). The global hypoxic volume (here defined as the volume of water masses with O_2 concentration below 40 mmol/m^3) from the observation is around 45.5×10^{15} m^3 and most of the model overestimates the hypoxic volume compared to observations (see Table 2). MITgcm-CTL simulates a slight

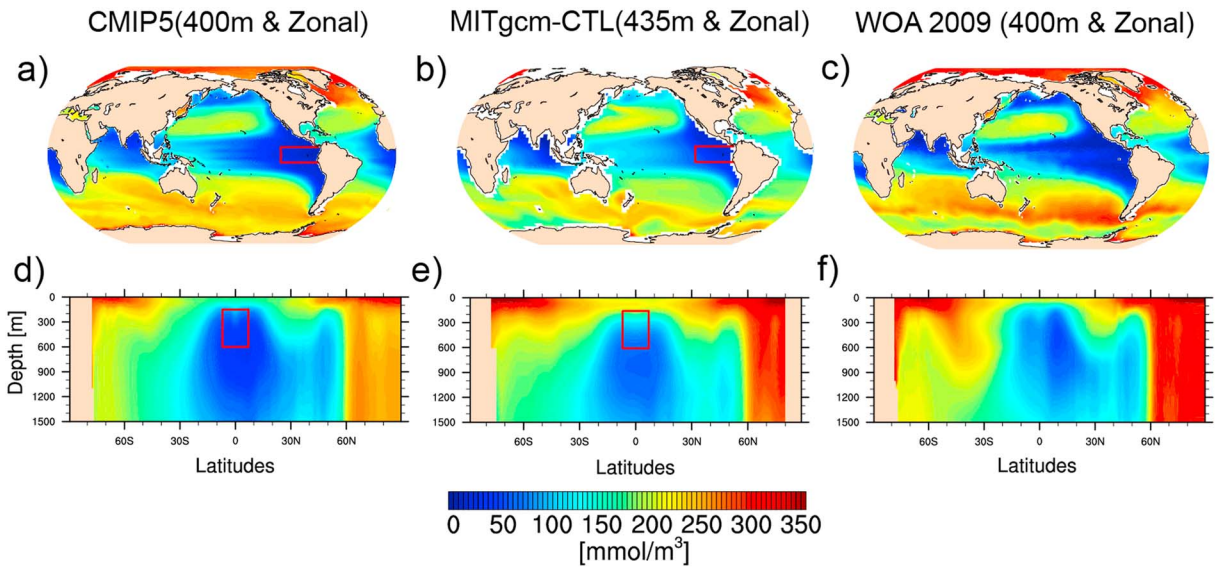

Figure 4. (a)–(c) Comparison of climatological annual mean dissolved oxygen concentration (mmol/m^3) at 400 m (435 m for MITgcm-CTL) and (d)–(f) zonal mean distributions from CMIP5 multimodel mean data, MITgcm-CTL (control run), and WOA2009. Climatology from the model is based on the 30-year mean in the late twentieth century (1971–2000). The red rectangular boxes in (a), (b) and (d), (e) show control volumes for calculating weighted volume mean time series in later analyses (area of the box domain 119–69°W, 7°S–7°N). CMIP5 = Coupled Model Intercomparison Project Phase 5; WOA2009 = World Ocean Atlas 2009; MITgcm-CTL = Massachusetts Institute of Technology general circulation model control experiments. This figure has been drawn by the NCL (The NCAR Command Language (Version 6.3.0), 2016).

underestimation in hypoxic volume, which is closer to the lower end of CMIP5 models (such as HADGEM2-ES in this case). This could be partly due to the strong vertical mixing in our model, ventilating more oxygen into the interior ocean.

3.2. Centennial Changes in O_2

The CMIP5 models predict a global deoxygenation under a warming climate with significant model-to-model differences in regional features (Bopp et al., 2013; Cabré et al., 2015; Cocco et al., 2013). We briefly examine the centennial changes in O_2 from CMIP5 models and compare it to our sensitivity experiments. Estimates of long-term changes are calculated as the epoch difference between the 30-year averages from the early twentieth century (1901–1930) and the end of the 21st (2071–2100). To analyze the factors contributing to changes in O_2, we partitioned O_2 changes into two components. The thermodynamically driven component, oxygen solubility ($O_{2,sol}$), primarily depends on temperature (θ; but also on salinity, S), and the biologically driven component, apparent oxygen utilization (AOU), represents the cumulative loss of O_2 due to respiration.

$$O_2 = O_{2,sol}(S, \theta) - AOU. \quad (1)$$

Table 2
Evaluations of Climatological (1971–2000 Long-Term Mean) O_2 Metrics Between CMIP5 Models, MITgcm-CTL, and Observations (World Ocean Atlas 2009). The Top Two Rows Show the Global Mean Bias and the Global Spatial Correlation (R) Between the Model Outputs and Observational Patterns of Dissolved Oxygen at 400 m (435 m for MITgcm-CTL)

	GFDL-ESM 2 M	GFDL-ESM 2G	HADGEM2-ES	IPSL-CM5A-MR	MPI-ESM-MR	CESM1-BGC	CMIP5-MEAN	MITgcm-CTL
Global ΔO_2	−7.23	−18.45	+7.76	+13.63	−5.05	−30.94	−3.39	−17.79
Global-*R*	0.88	0.90	0.90	0.93	0.93	0.87	0.96	0.90
Pacific ΔO_2	+28.06	−6.1	+21.09	+30.98	−18.46	−42.96	+1.62	+21.3
Pacific-*R*	0.77	0.89	0.81	0.88	0.87	0.90	0.93	0.85
Global vol40 [×10^{15} m^3]	95.1	104.1	10.7	150.6	113.8	64.7	45.8	34.6

Note. The next two rows show the same as the first two rows except for the Pacific Ocean (north of 20°S). The bottom row shows the global hypoxic volume (in 10^{15} m^3) based on the criteria of 40 mmol/m^3. ESM = Earth System Model; CMIP5 = Coupled Model Intercomparison Project Phase 5; MITgcm-CTL = Massachusetts Institute of Technology general circulation model control experiments.

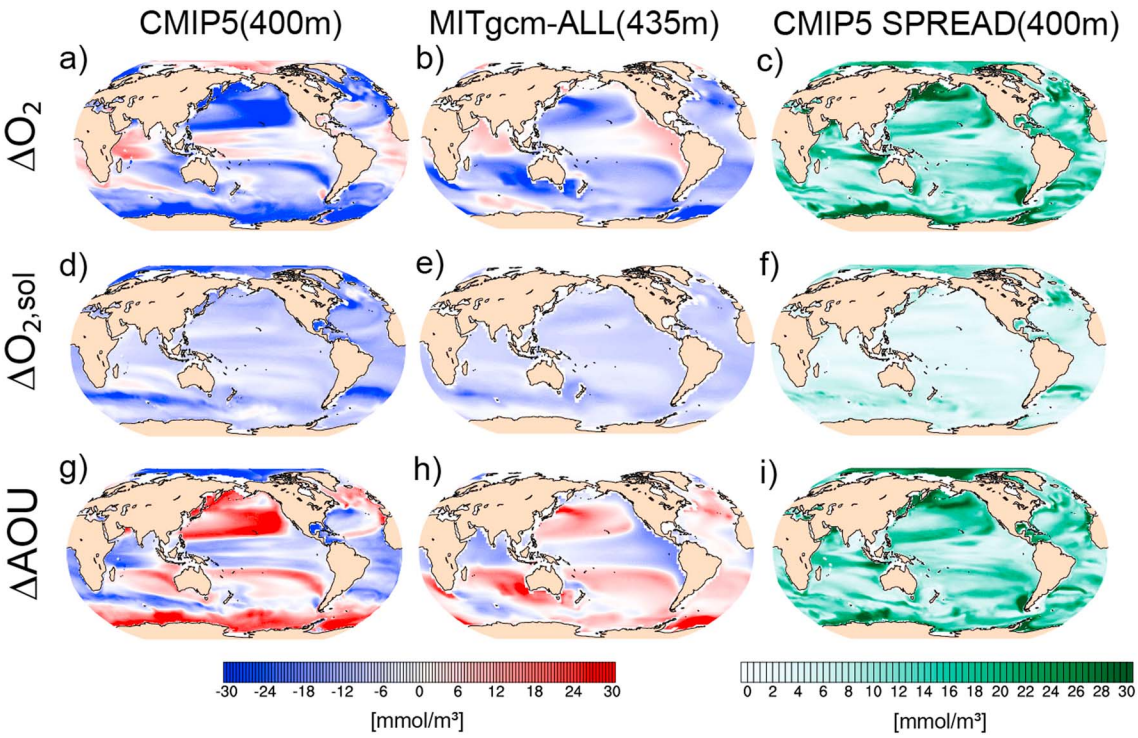

Figure 5. Changes in (a, b) dissolved oxygen (ΔO_2), (d, e) oxygen solubility ($\Delta O_{2,sol}$), and (g, h) ΔAOU, based on (a, d, g) CMIP5 multimodel mean under the RCP 8.5 scenario, (b, e, h) MITgcm-ALL (i.e., difference between sensitivity experiments with all climatic forcing and control run), and (c, f, i) CMIP5 multimodel spread based on ΔO_2, $\Delta O_{2,sol}$, and ΔAOU from selected CMIP5 models (see Table 1). Calculations in (a), (d), and (g) are the epoch differences between the temporal mean from 1901–1930 and 2071–2100 mean. AOU = Apparent Oxygen Utilization; CMIP5 = Coupled Model Intercomparison Project Phase 5; MITgcm-CTL = Massachusetts Institute of Technology general circulation model control experiments. This figure has been drawn by the NCL (The NCAR Command Language (Version 6.3.0), 2016).

The AOU approximates the effect of cumulative biological utilization, but it may also include the effects of air-sea disequilibrium and diapycnal mixing (Ito et al., 2004). Its changes over time can be influenced by changes in circulation as well as respiration rates.

Long-term changes in the thermocline O_2, $O_{2,sol}$, and AOU in MITgcm-ALL are comparable in magnitude to the multimodel mean of CMIP5 (Figure 5). In most of the midlatitude to high-latitude regions, including the North Pacific and Atlantic, and the Southern Ocean, O_2 decreases in CMIP5 models and MITgcm-ALL (Figures 5a and 5b). The magnitude of local O_2 changes differs among the models by ±30 mmol/m^3 (see CMIP5 spread from Figure 5c) but the centennial decrease in the extra-tropical thermocline is a robust feature as previously discussed (Bopp et al., 2013; Cabré et al., 2015; Cocco et al., 2013). The behavior of O_2 changes in tropical oceans differs from that of midlatitude to high-latitude regions as also discussed by previous studies (Bopp et al., 2013, 2017; Cabré et al., 2015; Cocco et al., 2013). Most CMIP5 model projections show no change or even a slight increase in the thermocline O_2 over the tropical oceans (Figure 5a). Previous modeling studies showed an increase in the tropical thermocline O_2 under a global warming scenario (Matear & Hirst, 2003). The MITgcm-ALL (Figure 5b) also exhibits an increase of the tropical thermocline O_2 even though simulations are conducted with a relatively simple climatic forcing. In the eastern tropical Pacific Ocean and Indian Ocean, MITgcm-ALL O_2 increases by about 10 mmol/m^3. We note that the magnitude of the O_2 increase is overall larger in the eastern tropical Pacific Ocean compared to the CMIP5 multimodel mean (Figures 5a and 5b) but some models show an O_2 increase comparable in magnitude to that of MITgcm-ALL (figure not shown). Despite detailed differences in the spatial patterns of the CMIP5 model projections and MITgcm-ALL, tropical thermocline O_2 is relatively stable in the warming world. The cause of relatively stable tropical O_2 inventories could be further explained by decomposing the O_2 changes into thermodynamically and biologically driven components.

Temperature increases result in a decrease in $O_{2,sol}$ as shown by both the CMIP5 multimodel mean projections and MITgcm-ALL (Figures 5d and 5e). Overall, the strongest decrease of $O_{2,sol}$ occurs in midlatitude

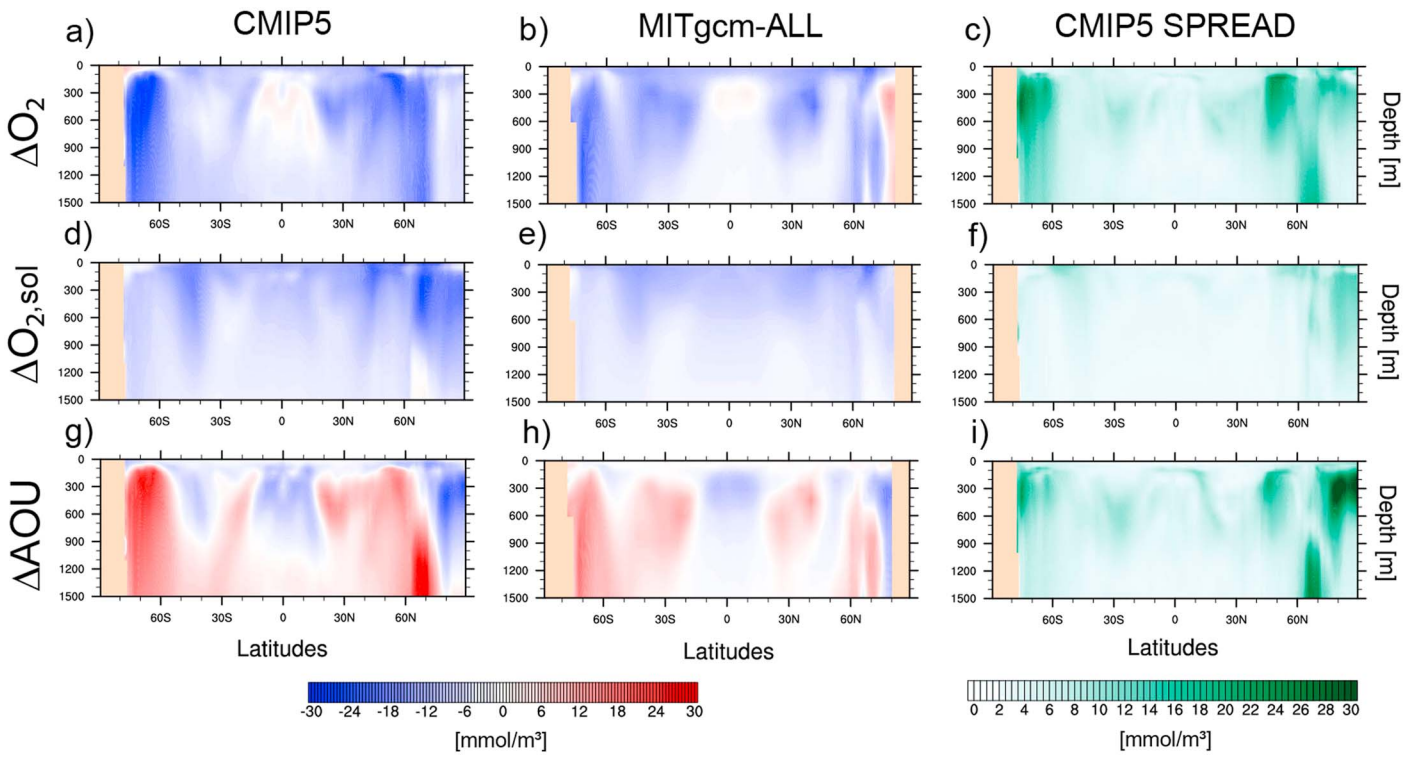

Figure 6. The same as in Figure 5 except for zonal mean. AOU = Apparent Oxygen Utilization; CMIP5 = Coupled Model Intercomparison Project Phase 5; MITgcm-CTL = Massachusetts Institute of Technology general circulation model control experiments. This figure has been drawn by the NCL (The NCAR Command Language (Version 6.3.0), 2016).

regions such as the North Pacific and the Southern Ocean. While the centennial changes in O_2 are relatively small in the tropical thermocline (Figures 5a and 5b), the $O_{2,sol}$ decreases are almost spatially uniform (Figures 5d and 5e). Thus, the changes in AOU must explain the apparent decoupling between O_2 and $O_{2,sol}$ in the tropics. The CMIP5 multimodel mean projections show an increase in AOU in midlatitude to high-latitude oceans (Figures 5g and 5h) likely due to the reduced ventilation (Cabré et al., 2015; Keeling et al., 2010). The spread in O_2 changes could also be mainly explained by the spread in AOU in midlatitude to high-latitude regions, and the spread of changes in $O_{2,sol}$ are relatively small (Figures 5f and 5i). In contrast, changes in thermocline AOU show relatively stable or decreasing values in the tropics for the CMIP5 multimodel mean (Figure 5g). However, the sign of oxygen changes in the eastern tropical Pacific is different in most of the CMIP5 models. While our model's response is strong compared to the CMIP5 in this region (Figures 5a and 5b), it is within the range of the spread within the CMIP5 models. Tropical oxygen is difficult to model because the changes in the solubility and AOU are of the same sign and of similar magnitude. After the compensation, the net O_2 change seems to be set by the relatively small residual, thus we see different signs of response among the models. While the temperature is increasing, and the increase in AOU tends to reinforce the O_2 decline in the midlatitudes, they cancel one another to moderate the O_2 change in the tropics, which is consistent with previous ESM studies (e.g., Bopp et al., 2013, 2017). This feature is also reproduced by the MITgcm-ALL experiment (Figure 5h).

The zonal mean centennial changes in O_2 reveal the vertical extent of thermocline O_2 changes, with some common features between the CMIP5 multimodel mean projection and MITgcm-ALL (Figure 6). O_2 in the upper 1,000 m decreases in most of the regions except in the tropical oceans (between 20°S–20°N). Differences in the spatial pattern of warming and thus $O_{2,sol}$ between the CMIP5 models and MITgcm are possibly due to the simpler SST forcing and the differences in background vertical mixing parameterization applied to our simplified model (Figures 6d and 6e). Reduced ventilation tends to decrease the subduction of water masses from the surface into the interior ocean and results in an AOU increase in middle to high latitudes in the upper water column (Figures 6g and 6h). However, as our analysis and previous studies mentioned, AOU tends to decrease in tropical oceans and this decrease is especially strong in the core of the

OMZs (i.e., depth between 200 and 800 m). The zonal mean change in O_2 also highlights the difference between middle to high latitudes and low latitudes, where we observe opposing changes in AOU.

Despite its simplicity, the MITgcm-ALL reproduces the key contrast between the tropics and midlatitude to high-latitude differences in O_2 changes from the CMIP5 models. It is important to note that the basin-scale response of AOU to the warming climate is not identical among the individual CMIP5 model projections, nor between the MITgcm-ALL and the CMIP5 multimodel mean. Next, we further analyze the simulations from sensitivity experiments seeking to understand some of the mechanisms at work that are common among the CMIP5 model projections. In the next sections, we will use the different MITgcm experiments to determine which components of climate forcing control the projected decline of tropical AOU.

4. Mechanisms of Centennial-Scale O_2 Change in the Tropical Pacific Thermocline

4.1. Tropical Pacific Thermocline O_2 Changes

Previous studies have shown that the CMIP5 model projections show significant model to model differences in the tropical O_2 changes on the centennial timescale where even the sign of the changes is not in agreement (Bopp et al., 2013, 2017; Cabré et al., 2015; Cocco et al., 2013). The tropical O_2 changes may be highly uncertain and model-dependent because the net O_2 change results from a slight imbalance between the two, mostly compensating factors: $O_{2,sol}$ and AOU as also mentioned in previous studies. In this section, we focus on the changes in the thermocline (150–600 m) O_2 in the eastern tropical Pacific Ocean as it hosts the largest OMZ in the global ocean. We compare the evolution of O_2, $O_{2,sol}$, and AOU (in the eastern tropical Pacific Ocean) over time from selected CMIP5 models and the MITgcm-ALL experiment, as well as from each sensitivity experiment (details in section 2.4).

Majority of the CMIP5 models (all but the IPSL-CM5A-MR) show no change or an increase in O_2 under the warming climate. All of the models, including our sensitivity experiments, show a decrease in $O_{2,sol}$ of 6–15 mmol/m^3 due to the effect of warming (Figures 7c and 7d). Most of the models project decreasing AOU (again except for the IPSL-CM5A-MR) which results in an opposite tendency of tropical Pacific O_2. Cabré et al., 2015 also mentioned the exception of IPSL's model response, which could be because of a decrease in ventilation within the anoxic regions. How does each aspect of climate forcing (i.e., warming, changes in the hydrological cycle, and surface winds) impact tropical Pacific thermocline O_2? Our sensitivity experiments highlight the importance of ocean warming, which results in opposing changes in $O_{2,sol}$ and AOU (Figures 7d and 7f). This is also implied by ESM studies of Gnanadesikan et al. (2007). Changes in the hydrological cycle and tropical Pacific trade winds play a secondary role in decreasing AOU, but their overall magnitude is small. The response of O_2 and AOU to changes in tropical Pacific trade winds is weak compared to the previous studies of Ridder and England (2014). We note that the tropical Pacific trade wind forcing used in their studies is highly idealized, changing the wind stress between 30°S and 30°N in various magnitudes. Our localized and weaker forcing based on CMIP5 future projections could be the cause of weak O_2 and AOU response. The slight increase in O_2 due to positive trend of the SAM could be originated from the more oxygen-rich intermediate water mass supply from the Southern Ocean indicated by previous studies (e.g., Getzlaff et al., 2016). We note that the MITgcm-SAM in our study is not the same as the sensitivity experiments from Getzlaff et al. (2016) for two aspects. First, they used a simple coupled model applying RCP8.5 CO_2 emissions and then conducted the Southern Ocean wind sensitivity experiments on top of the simple coupled simulations. This means that they explored the sensitivity to wind on top of the atmospheric warming. The second aspect is that they included additional parameterization of the unresolved equatorial current system by adding high values of zonal isopycnal diffusion coefficients in the equatorial region (Getzlaff & Dietze, 2013). This could potentially change the transport of water mass, which could alter the O_2 response to climatic change and this type of additional parametrization is not included in CMIP5 simulations.

Despite the differences in parameterizations, our study and previous studies (e.g., Getzlaff et al., 2016; Oschlies et al., 2018) both suggest that the changes in wind stress patterns and magnitudes act on O_2 in a very sensitive manner, which could be one of the potential sources of diverse response and bias in O_2 changes among the ESMs. In the next section, we examine the mechanistic link between the ocean warming and the decline of AOU.

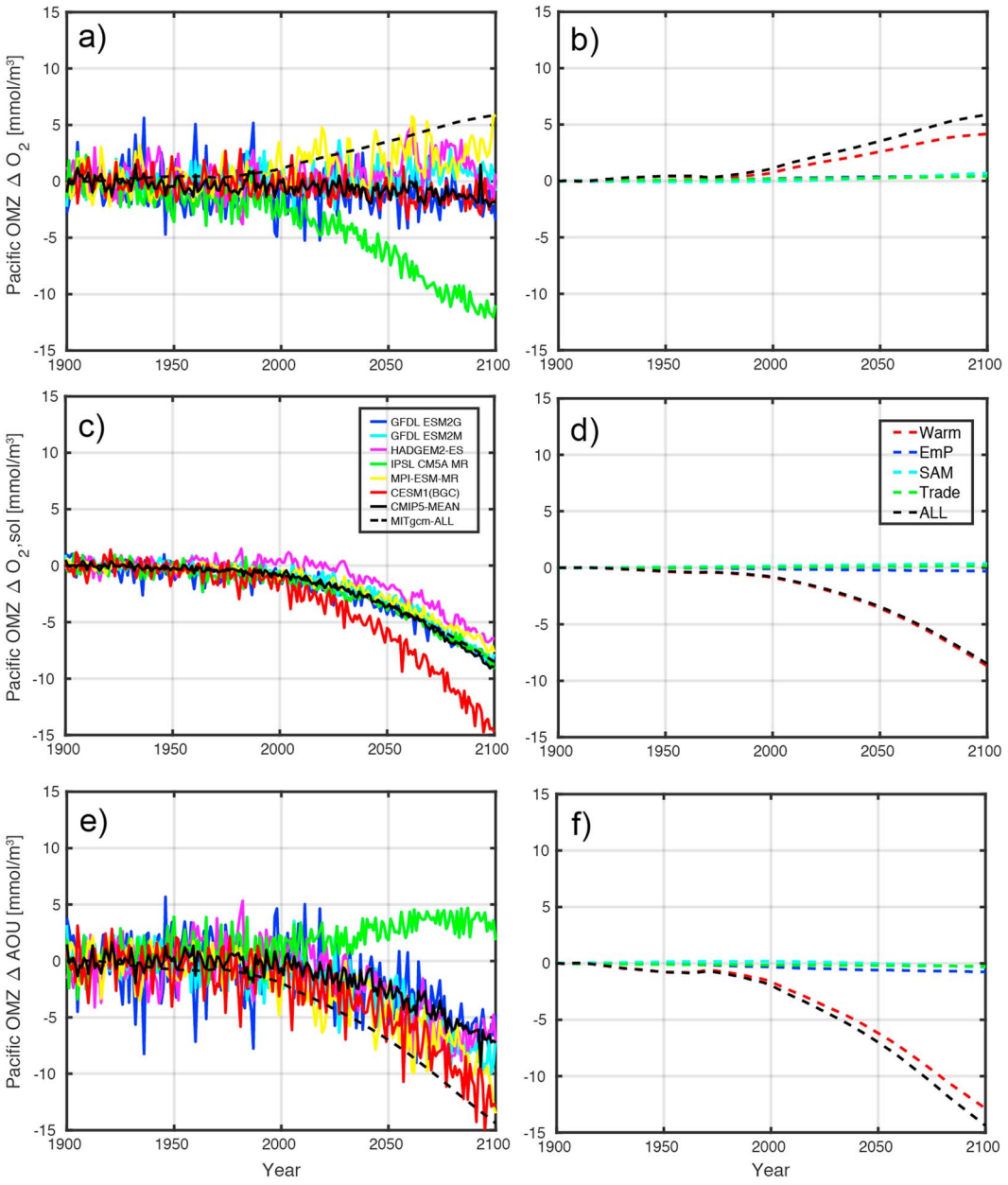

Figure 7. Temporal evolution of weighted area-mean thermocline properties averaged over the eastern tropical Pacific Ocean from 150–600 m (160–610 m) depth (rectangular boxes shown in Figures 4a and 4d), from (a, c, e) CMIP5 models (including MITgcm-ALL) and (b, d, e) a suite of perturbation experiments: (a, b) dissolved oxygen, (c, d) oxygen solubility, and (e, f) AOU time series from CMIP5 models are based on anomalies relative to averaged values from 1901–1930. (b, d, e) as in (a, c, e) except for sensitivity experiments based on MITgcm, shown as the deviation from the control experiment. All data are in mmol/m^3. OMZ = Oxygen Minimum Zone; AOU = Apparent Oxygen Utilization; ESM = Earth System Model; CMIP5 = Coupled Model Intercomparison Project Phase 5; MITgcm = Massachusetts Institute of Technology general circulation model; SAM = Southern Annular Mode.

4.2. Causes of the Centennial Decline in the Low-Latitude AOU: Export Production

There are two primary mechanisms that may cause tropical Pacific AOU to decline: (1) reduced rates of organic matter decomposition and (2) younger age of waters in the tropical thermocline. The water mass age measures the length of time the parcel has spent in the interior ocean since the last contact with the surface mixed layer. In this section, we focus on (1) the organic matter decomposition. As a metric of the organic matter decomposition, we examine the export flux of particulate organic matter at around 100 m depth.

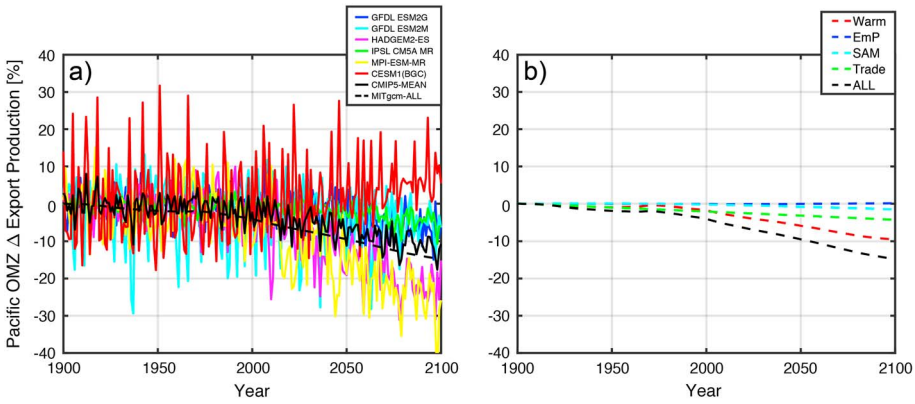

Figure 8. Fractional changes in the eastern tropical Pacific Ocean (box shown in Figure 4) export production at 100 m (116 m for MITgcm). Fractional changes are shown in (a) from the CMIP5 models relative to the average values of export production from 1901–1930, and in (b) from the sensitivity experiments, relative to the control experiment (red: warming; blue: freshwater: light blue: The Southern Ocean wind; green: tropical trade wind; yellow: off-equatorial wind; and black dashed: all forcing). OMZ = Oxygen Minimum Zone; ESM = Earth System Model; CMIP5 = Coupled Model Intercomparison Project Phase 5; MITgcm = Massachusetts Institute of Technology general circulation model; SAM = Southern Annular Mode.

Since most sinking organic matter is oxidized at depths shallower than 1,000 m, the reduction of particle flux translates into slower respiration rates in the thermocline. The CMIP5 model projections show significant reductions in the globally integrated export production in the range of 5–20% (regionally up to 40%) by 2100 (Bopp et al., 2013, 2017). The decrease of export production occurs globally except for the polar latitudes influenced by the reduction of sea-ice cover and mixed layer shoaling. In the eastern tropical Pacific Ocean, the regional decline of export production is more pronounced than the global mean, in the range of 10–30% reduction by 2100 (Figure 8a). Thus, the reduced AOU could partially be caused by the declining biological productivity and subsurface respiration. We note that most of the CMIP5 models include denitrification. In our model, remineralization turns off when O_2 draws down to certain threshold, but fixed nitrogen is not removed. Centennial changes in export production will not fully translate into oxygen consumption since denitrification dominates more in O_2 deficit regions. Therefore, we cannot compare changes in anoxic zone to geochemical isotope proxies for centennial changes in denitrification rates (Deutsch et al., 2014). Uncertain relationships between export production and AOU from CMIP5 models could also depend on these processes (Bopp et al., 2017).

The MITgcm-ALL projects approximately 15% decline of export production (Figures 8a, ALL, and 8b), primarily driven by the effect of ocean warming (~10%). The slackening of the easterly trade winds also plays a secondary role in reducing the amount of export production (~5%). The decline of export production due to weakening of trade winds is consistent with the previous study of Ridder and England (2014), but again, the weak response compared to the Ridder and England (2014) could be due to weak and localized changes in tropical Pacific winds. Increased stratification as well as weakened wind-driven upwelling decreases the supply of nutrients to the surface of the tropical Pacific Ocean, reducing the amount of sinking organic matter and subsurface O_2 consumption. When all the climatic forcing is applied together, the export production decreases slightly more than the sum of the individual effect, implying a weak nonlinear effect.

4.3. Causes of the Centennial Decline in the Low-Latitude AOU: Water Mass Age

In this section, we will further diagnose how individual climatic forcing could modulate the ideal age on centennial timescales based on sensitivity experiments, which is difficult in general to diagnose from CMIP5 models. The climatological zonal mean ideal age exhibits latitudinal differences in vertical distributions. Low age water mass penetrates more into the interior ocean in midlatitude to high-latitude close to 900 m (Figure 9a). In contrast, the vertical age gradient is higher in the upper ocean (300–500 m) in the tropics, which indicates that changes in upwelling could have significant impact on water mass composition in the OMZs. The zonal mean changes in ideal age from the sensitivity experiments reveal a strong latitudinal

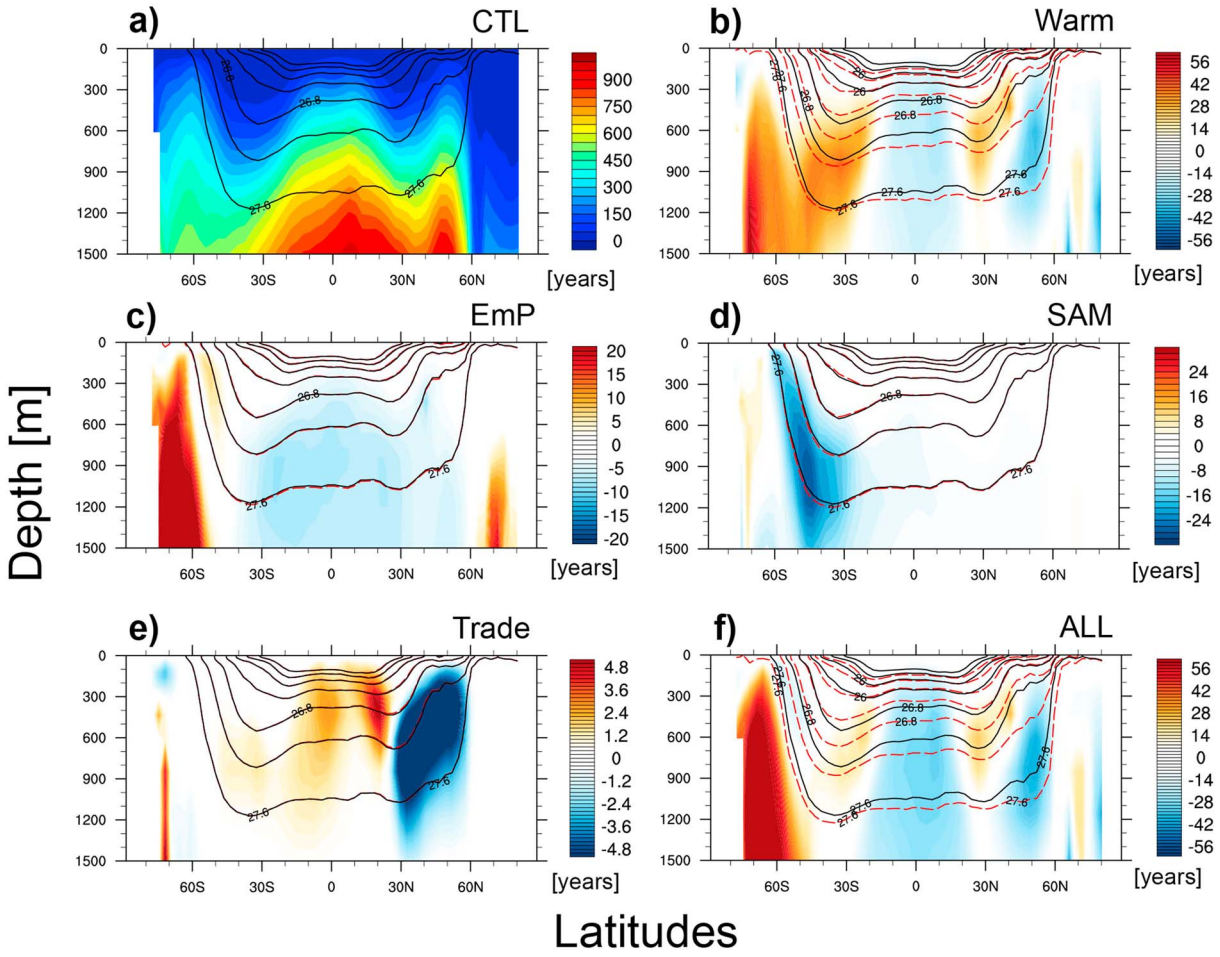

Figure 9. The zonal mean distributions of ideal age (control and anomalies) based on MITgcm sensitivity experiments ((a) from control experiment, not anomaly; (b) warming; (c) hydrological cycles; (d) the SAM wind stress; (e) tropical trade winds; (f) all forcing). The plots from (b)–(f) depict the anomaly from the MITgcm-CTL (a), with the ideal age anomaly (shading) and changes in potential density (dotted contours; MITgcm-CTL in black-solid contours and sensitivity experiments in red-dashed contours). Note that each color bar has a different scale. SAM = Southern Annular Mode; MITgcm-CTL = Massachusetts Institute of Technology general circulation model control experiments. This figure has been drawn by the NCL (The NCAR Command Language (Version 6.3.0), 2016).

difference in changing the age of water mass by the end of the century (Figures 9b–9f). Older age reflects relatively weak ventilation leading to increased cumulative consumption of O_2 there if the rate of organic matter decomposition remains the same. When all climatic perturbations are imposed, strong negative anomalies of ideal age occur over the tropics in the subsurface ocean (200–1000 m; Figure 9f, ALL). Surface climate forcing alters the ventilation rates and pathways of the thermocline waters (e.g., Gnanadesikan et al., 2012). Positive anomalies of ideal age occur at midlatitudes and in the Southern Ocean. The reduced age in the tropical oceans are due to the combined effects of ocean warming and enhanced freshwater forcing but contributions from warming dominates (Figures 9b, 9c, and 9f, Warm, EmP, and ALL). Potential density decreases throughout the upper 1,000 m, as we expected from the effect of warming, with a ~0.3 kg/m^3 decrease of potential density near the depth of OMZs in the tropics. The ideal age increases due to the freshwater forcing (Figure 9c, EmP) in the Southern Ocean, potentially linked to the suppressed deep convection (de Lavergne et al., 2014; Ito et al., 2015). On the other hand, the ideal age decreases in the southern midlatitudes due to enhanced ventilation driven by the intensification and poleward shift of zonal winds (Figure 9d). Reduction of the trade winds somewhat compensates the effects of increased thermal and haline stratification on the tropical thermocline. Changes in off-equatorial trade winds decrease the ideal age in northern midlatitudes due to changes in gyre circulations and upwelling. The effect of all forcings is a net decrease in the ideal age and AOU averaged over the tropical thermocline. The ideal age increase due to the changes in trade wind is also shown in the previous study (Ridder &

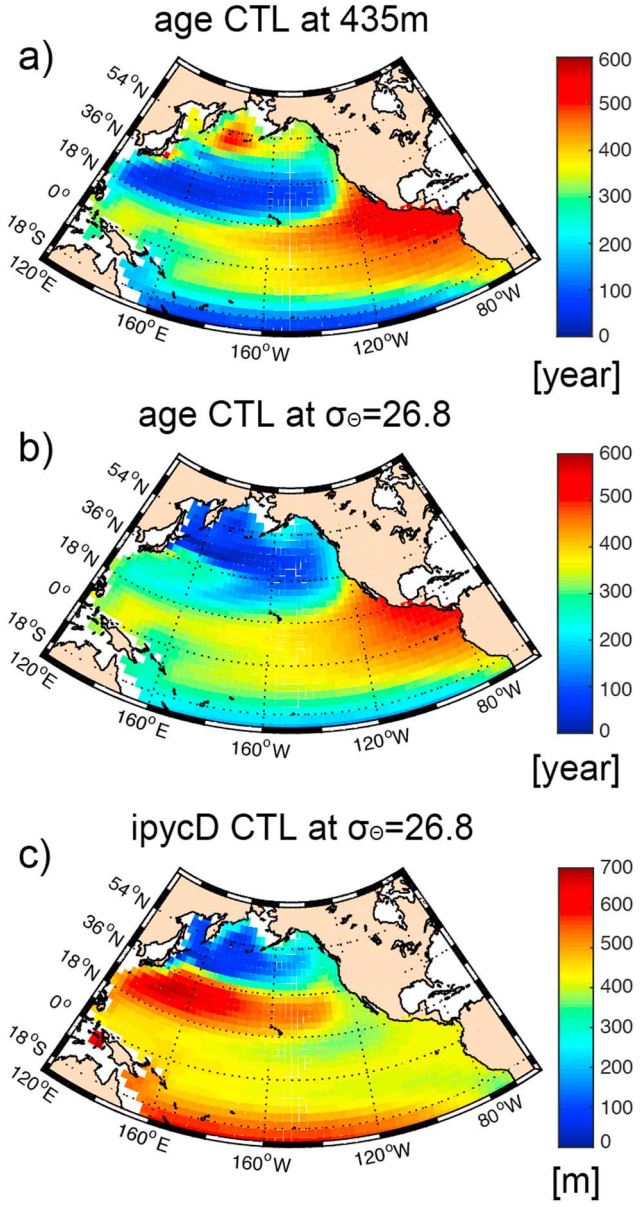

Figure 10. Distributions of ideal age (a) at 435 m, (b) on an isopycnal layer (at σ_θ = 26.8), and (c) on an isopycnal layer depth at σ_θ = 26.8 from the Massachusetts Institute of Technology general circulation model CTL. CTL = control experiments.

England, 2014). Again, we note that the forcing in their sensitivity experiments are highly idealized and does not include equatorial and off-equatorial wind stress perturbations in our experiments. The off-equatorial wind stress change results in ideal age decrease in off-equatorial Pacific (30–60°N) regions (Figure 9e). Sensitivity experiments indicate the dominance of the effect of ocean warming reducing the ideal age in the tropics, consistent with previous studies from Gnanadesikan et al. (2007). To highlight the changes in water mass age due to changes in upwelling from certain climate forcing, we further analyze the age in two different coordinates, depth and isopycnal coordinates.

We examine the changes in the ideal age at a constant depth (at 435 m) and on an isopycnal surface (at σ_θ = 26.8) in the Pacific basin. The depth and potential density values are chosen for their proximity to the OMZs of the tropical Pacific (Karstensen et al., 2008). Before looking at the climatic response in ideal age from sensitivity experiments, we will explore the climatological distributions of ideal age and isopycnal layer depth in the Pacific basin. The depth of the isopycnal layer varies from approximately 400 m in the tropics to deeper than 700 m in the western subtropics (Figure 10c). The isopycnal layer we chose here is close to the core of the OMZ in the tropical Pacific Ocean. Comparing the steady states (MITgcm-CTL) of ideal age between depth and isopycnal coordinates (Figure 10), the overall structure is similar between the two coordinates, where the ventilated subtropical thermocline is significantly younger than the unventilated tropical thermocline (Luyten et al., 1983). A strong gradient of the ideal age tracer exists at about 20°S and 20°N.

Ocean warming causes the most pronounced effect on ideal age in the North Pacific in the western boundary current region (Figure 11a). Ocean warming results in more than 50 years of decrease in the ideal age at 435 m in the tropical Pacific Ocean. Intensification of the hydrological cycle and Southern Ocean winds (Figure 11c) also contribute to the decrease of ideal age (~10 years in total) in the tropical Pacific but the magnitudes are small compared to the effect of ocean warming. Weakening of trade winds results in an increase in the ideal age (~10 years) in the tropical Pacific Ocean (included in Figure 11c). The off-equatorial surface westerly wind results in increasing ideal age at around 20°N in the Pacific Ocean (included in Figure 11c), which is also evident from the zonal mean distributions (see Figure 9). The net effect is a decrease in the ideal age at 435 m in the tropical Pacific Ocean, dominated by the response to warming.

In contrast, the ideal age on the isopycnal layer increases at all latitudes (Figure 11f). The effect of ocean warming contributes the most to the increase in ideal age. Its increase is the greatest in the subtropical gyre regions (by 150–200 years). Nonwarming effects decrease the ideal age tracer (~5 years) mainly because of the intensification of hydrological cycle and zonal winds in the Southern Ocean (included in Figure 11d). However, the magnitudes are much smaller compared to that of ocean warming. The weakening of trade winds in the tropical Pacific Ocean slightly reinforces the effect of ocean warming in increasing the ideal age in the eastern tropical Pacific (figure not shown).

Diagnosing the ideal age tracer on two different coordinates highlights different aspects of changes in water masses (Figure 11). In the interior ocean, the circulation is primarily oriented along isopycnal surfaces, and a reduced ventilation increases the isopycnal ideal age. In contrast, the changes in the ideal age of the tropical thermocline at a constant depth can be explained as the shift in the vertical advective-diffusive balance as discussed in Gnanadesikan et al. (2007). The warming could slow down the shallow overturning circulations, which could result in less old water injected from the deep ocean into the intermediate depths in the tropical Pacific Ocean (Gnanadesikan et al., 2007). Differences in coordinates highlight two distinct mechanisms,

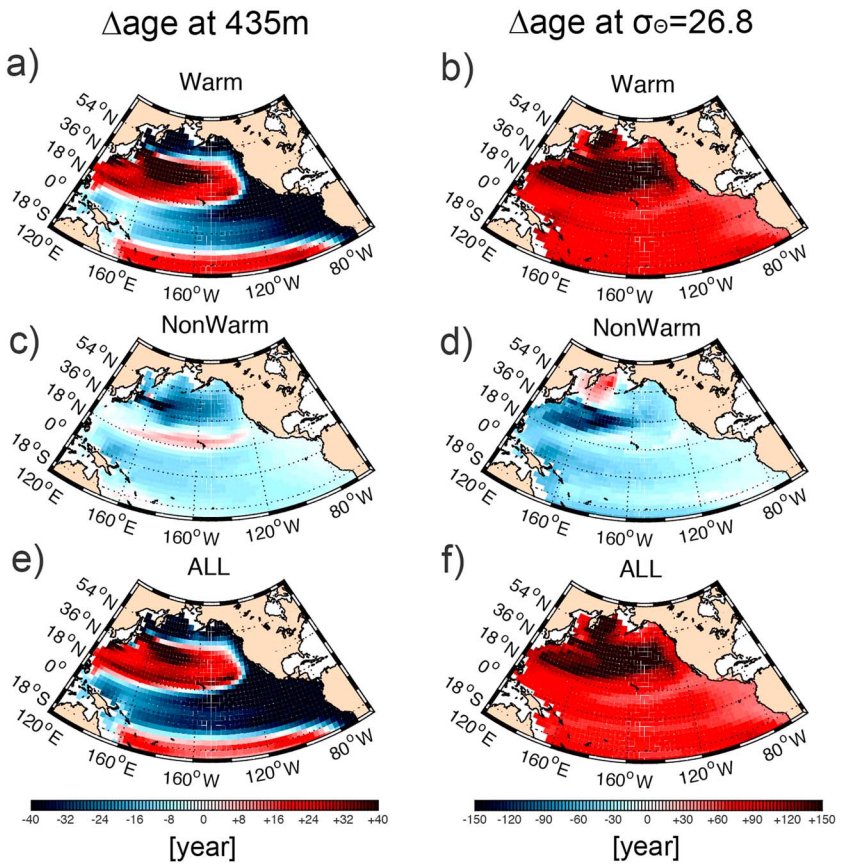

Figure 11. Changes in the ideal age tracer (a, c, e) at 435 m, (b, d, f) on the isopycnal layer at σ_θ = 26.8. The ideal age and isopycnal layer depth changes are anomalies from the control run. Warm is from the warming experiment and nonwarm is from the linear sum of hydrological cycles and wind stress change experiments. ALL is from the experiment including all climatic forcings.

which could result in differences in ideal age response particularly in the tropical Pacific Ocean (Figure 11). It is important to point out that the narrow jets in the equatorial Pacific Ocean are known to ventilate and supply oxygen to the eastern Pacific OMZs (Stramma et al., 2010), and these features are not fully resolved in CMIP5 and the MITgcm simulations. Thus, the current generation of climate models lacks an important process controlling the O_2 level of the tropical thermocline. The MITgcm experiments indeed reproduces the overall tropical and midlatitude to high-latitude contrast of the AOU change in the CMIP5 multimodel mean, and the underlying change in the water age is likely linked to the reduction in the isopycnal ventilation as well as the large-scale vertical shift in the water mass distributions. However, the effect of this water mass shift could be exaggerated in the MITgcm since the background vertical diffusion is relatively high and the mixing parameterization is simplified compared to CMIP5 models. Duteil and Oschlies (2011) showed changes in O_2 sensitivity to background mixing and conclude that higher vertical mixing could potentially result in expanding the suboxic zones. This is in opposite sense from our study. Overall the ideal age decreases in their simulations, which is consistent with our simulations. We hypothesize that the key difference is in the sensitivity of biological O_2 consumption to vertical mixing. Changes in export production can modulate the magnitude of O_2 change in the tropical Pacific Ocean under certain vertical mixing intensity. The sensitivity of export production differs between our simulations and studies of Duteil and Oschlies (2011). This can be an important source of uncertainty in O_2 changes among ESMs. In our simulations, the overall effect of changes in the ideal age wins and this could translate into higher decrease in AOU (i.e., increase in O_2) at certain depths, as we saw in a previous section (see Figures 5b and 5h). Vertical mixing and advection are critical in explaining these processes, and differences in how these processes are implemented in the model could result in diverse responses in O_2 and AOU changes on centennial timescales.

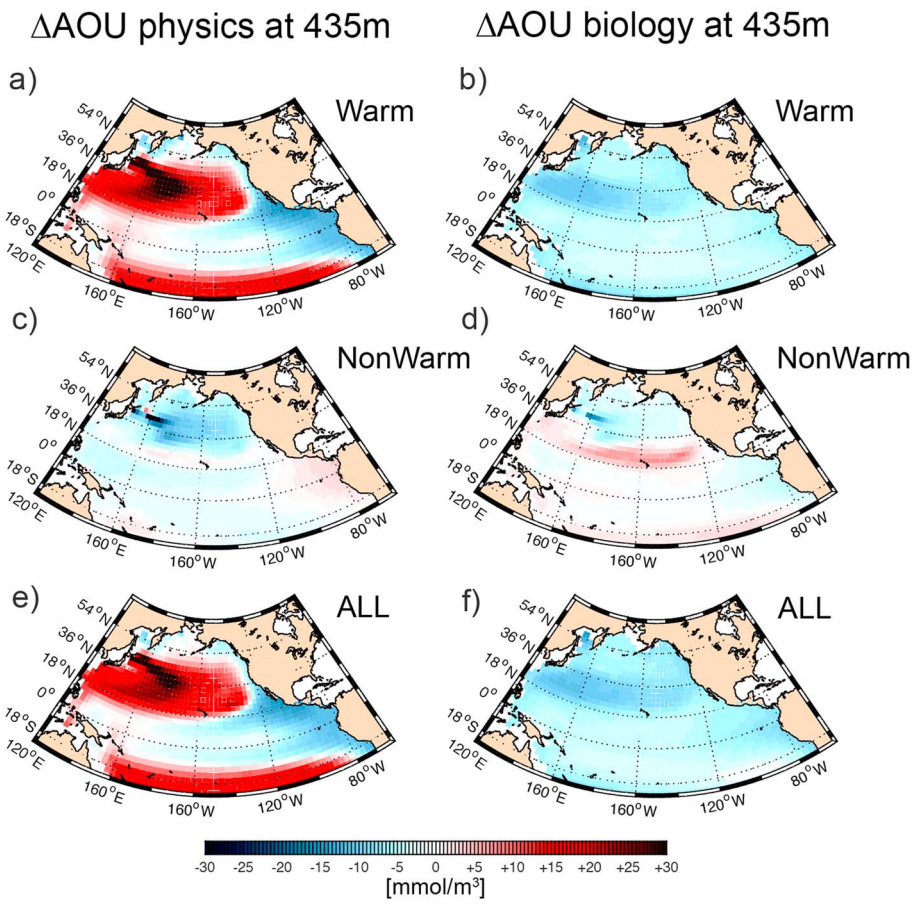

Figure 12. As in Figure 11 except for physically driven AOU (AOU_{phys}) and biologically driven AOU (AOU_{bio}) changes at 435 m. AOU = Apparent Oxygen Utilization.

4.4. Quantifying Physically and Biologically Driven AOU

The analysis of the ideal age tracer indicates the critical importance of the dependence of vertical coordinates in evaluating long-term O_2 changes as the water mass can shift significantly over centennial timescales. Water mass age and AOU have strong vertical gradients in the tropical thermocline, and the vertical water mass shift can cause significant changes. Here the remaining task is to quantitatively separate the two distinct causes of the AOU change from distinct climate forcing. As discussed in section 4.2, the export production in the tropical Pacific decreases primarily due to ocean warming (see Figure 8), which potentially reduces the oxygen utilization rate (OUR). At a constant depth, the vertical shift of water masses (Figure 11) could also reduce the water mass age and the AOU of the tropical thermocline. On a density surface, the deepening of the isopycnal due to ocean warming (see Figures 9b and 9f) can also decrease the OUR because the concentration of sinking organic matter decreases downward. Reduction in the export of organic matter and the downward displacement of isopycnal layers due to ocean warming could together decrease OUR, which could partially compensate the effect of weakened ventilation along the isopycnal surface.

To clearly and quantitatively separate the effects of different mechanisms behind the AOU change, we conduct additional sensitivity experiments. Our method of AOU decomposition is similar to the method developed by Deutsch et al. (2006). For each sensitivity run (A-E), an additional simulation is performed with a constant biological productivity, which is prescribed to the monthly mean climatology from the control experiment. To implement this, we first confirm that there is practically no model drift in the control simulation and record the monthly climatology of OUR from the control simulation. Then, the additional sensitivity runs are performed with the climatological OUR at each depth level. The climate change impacts on the OUR are suppressed in these experiments, thus isolating the circulation-driven AOU changes, ΔAOU_{phys}.

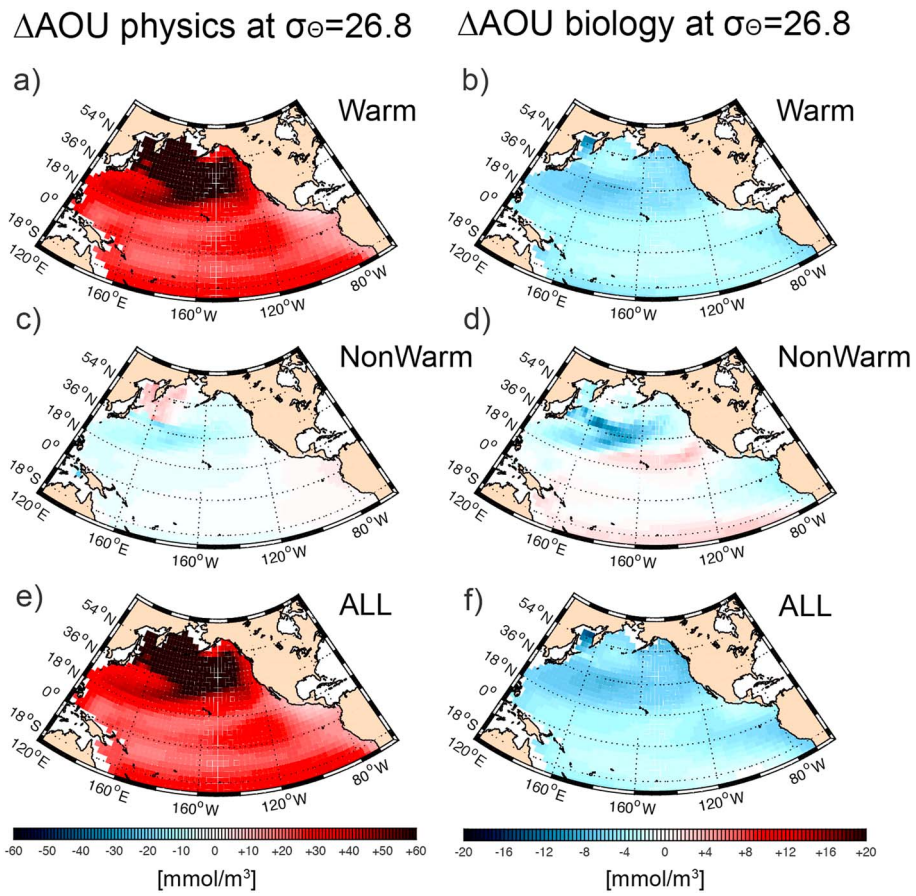

Figure 13. As in Figure 12 except on the isopycnal at σ_θ = 26.8. AOU = Apparent Oxygen Utilization.

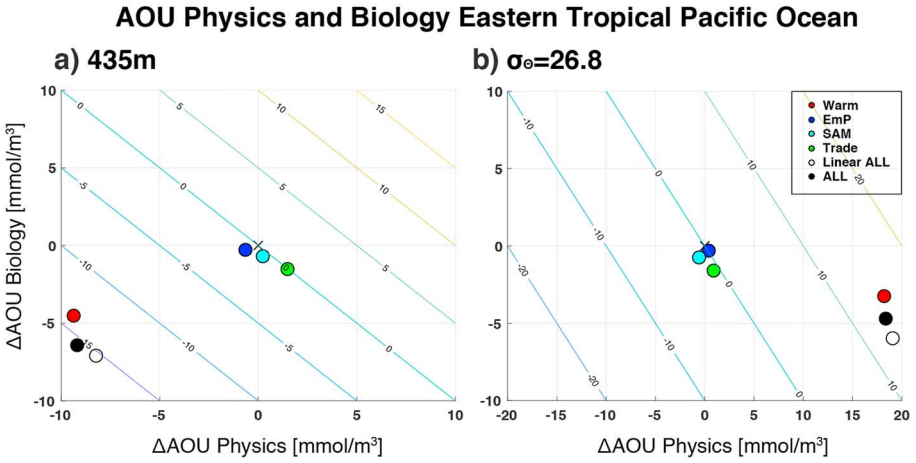

Figure 14. A phase diagram explaining ΔAOU as the sum of ΔAOU_{phys} (*x* axis) and ΔAOU_{bio} (*y* axis) in the eastern tropical Pacific Ocean (box shown in Figure 4) after 200 years of model integrations, for (left) 435 m and (right) along the isopycnal (σ_θ = 26.8). Weighted area-mean values from a suite of sensitivity experiments based on two different coordinates are plotted in colored dots. The nonlinearity is negligibly small (compare filled and open black circles). Colored contour lines indicate the total ΔAOU (ΔAOU_{phys} + ΔAOU_{bio}). The effects of the ocean heating and the trade wind explain most of the total ΔAOU. Note that the *x* axis range is different between the two panels. AOU = Apparent Oxygen Utilization; SAM = Southern Annular Mode.

Biologically driven AOU changes, ΔAOU_{bio}, can then be inferred by taking the residual between the total and the physically driven AOU changes assuming the linearity between the physically and biologically driven AOU.

$$\Delta AOU^{(n)} = \Delta AOU^{(n)}_{phys} + \Delta AOU^{(n)}_{bio}, \quad (2)$$

where the superscript *n* indicates the climate forcings (A-E) described in section 3.2. We diagnosed ΔAOU_{phys} and ΔAOU_{phys} from each sensitivity experiment. Figures 12 and 13 show the spatial pattern of ΔAOU_{phys} and ΔAOU_{bio} at the 435 m depth and on the $\sigma_\theta = 26.8$ surface. The pattern of ΔAOU_{phys} shows a strong increase in the subtropical oceans reflecting the weakened ventilation of thermocline waters (Figure 14e). ΔAOU_{phys} in the tropical Pacific Ocean shows a difference between the depth and isopycnal coordinates: it decreases at the 435 m depth but it increases on the σ_θ = 26.8 surface. The patterns of ΔAOU_{phys} (Figure 13, left panels) essentially mirror those of ideal age shown in Figure 11. The apparent decrease of ΔAOU_{phys} at 435 m is explained by the reduction of the water age due to the deepening of isopycnal layers. In contrast, ΔAOU_{bio} uniformly decreases both at the 435 m depth and on the σ_θ = 26.8 surface, due to the reduced biological oxygen consumption (right panels in Figures 12 and 13). Generally, the magnitude of ΔAOU_{bio} is smaller than ΔAOU_{phys}, so the net change in AOU is dominated by the physically driven changes.

Relative magnitudes of ΔAOU_{phys} and ΔAOU_{bio} can be visualized in a phase diagram (Figure 14) where the horizontal and vertical axes measure spatially averaged ΔAOU_{phys} and ΔAOU_{bio} in the eastern tropical Pacific thermocline (shown as the rectangular box in Figure 4) in the two vertical coordinates. At 435 m depth, ocean warming decreases AOU (Figure 14a) through reduction in both AOU_{phys} (by about 9 mmol/m^3) and AOU_{bio} (close to 5 mmol/m^3), leading to a total AOU decrease of about 14 mmol/m^3. Physically and biologically driven AOU have almost equal contributions to the decrease in AOU at constant depth. On the $\sigma_\theta = 26.8$ surface (Figure 14b), the effect of ocean warming increases ΔAOU_{phys} (close to 20 mmol/m^3), by about two times the magnitude as at 435 m (Figure 14a). The effect of ocean warming decreases ΔAOU_{bio} due to the reduced export production, but its contribution is minor in comparison to the physically driven changes. The warming-induced ΔAOU_{phys} dominates the AOU change in the isopycnal coordinate.

5. Summary and Discussion

We investigated the role of different surface climate forcing contributing to centennial changes in the thermocline O_2 and analyzed the underlying mechanisms using CMIP5 ESMs and an ocean general circulation and biogeochemistry model. Future projections from CMIP5 ESMs and a suite of sensitivity experiments using MITgcm illustrate the dominant patterns in the evolution of thermocline O_2 under a warming climate. Tropical thermocline O_2 inventory exhibits a small change as shown by several previous studies (Bopp et al., 2013, 2017; Cabré et al., 2015; Cocco et al., 2013). We conducted a suite of sensitivity experiments to decompose and quantify the simulated O_2 changes into the effects of various climatic forcings, mimicking the centennial climate change projection in the CMIP5 ESMs. The changes in the tropical Pacific thermocline O_2 content are relatively small due to the compensation between decreasing solubility and decreasing AOU driven by ocean warming. Changes in hydrological cycles and wind stress play a minor role on controlling the evolution of O_2 and AOU but the changes in ocean circulations and O_2 are very sensitive to changes in wind stress patterns and magnitude, which needs further investigation using different complexity of models. The decreasing AOU in the tropical thermocline is caused by the combination of weakened export production and the penetration of younger O_2-rich surface water through vertical transport, consistent with findings from previous ESM studies (Gnanadesikan et al., 2007). Our results indicate that this vertical transport alternation due to warming is likely to happen among CMIP5 models despite the differences in parameterization in diapycnal mixing processes. In the tropical Pacific, the AOU appears to decrease at a constant depth by sampling progressively lighter and younger water masses due to reduction in upwelling of deep water masses. We further quantified physical and biological aspects of AOU contributing to a decrease in centennial AOU in the tropical Pacific Ocean. The decrease of physical aspects (i.e., water mass age) accounts for about 43% of total AOU decrease, and biological aspects (i.e., the reduction of export production) accounts for about 57% of total AOU decrease in the tropical Pacific thermocline.

Similar findings from the CMIP5 models support a common mechanistic explanation, but we must be aware of some uncertainties and open questions associated with coarse-resolution models. The relatively low

resolution of these models does not fully represent the tracer transport of the equatorial current system, ocean eddies, and small-scale mixing processes. These unresolved physical processes have been implicated in the biases in the mean state of coarse models, but their impact on the response of OMZ ventilation and productivity to climate change remains unclear. The simple and relatively high vertical diffusion, particularly in the tropical oceans, could result in a stronger response in AOU (and water mass age transition) in our model compared to CMIP5 models. However, the latitudinal contrasts in AOU changes remains among CMIP5 models, which indicates that even with a more realistic background vertical diffusion, one-dimensional processes could still alter the AOU (and O_2) in the tropical oceans in an unexpected way under a warming climate. Similarly, the crude representations of biological processes and export production in current models may also neglect important mechanisms influencing O_2. For example, variations in organic matter stoichiometry can influence the size of the OMZ (DeVries & Deutsch, 2014) and its response to rising CO_2 (Oschlies et al., 2008). Second, the depth scale of organic matter respiration has been shown to vary with temperature (Weber et al., 2016). Neither of these are accounted for by current models and would alter ΔAOU_{bio}. Further studies with more sophisticated physical, ecological, and biogeochemical models may change the future O_2 projections in unexpected ways.

Significant decreases in global and regional O_2 and the expansion of OMZs are documented in historic data sets from the past several decades (Helm et al., 2011; Ito et al., 2017; Keeling et al., 2010; Schmidtko et al., 2017; Stramma et al., 2008, 2012), which may be dominated by interannual and decadal climate variability (Czeschel et al., 2012; Deutsch et al., 2011, 2014). The decadal-scale trends in the observations should not be confused with the century-scale projection of the ESMs that are potentially driven by different sets of mechanisms. Natural climate variability could significantly modulate O_2 concentrations on interannual to decadal timescales, which makes it a challenging task to detect long-term changes observationally (Long et al., 2016). Finally, this study mainly focused on the tropical Pacific Ocean but other tropical oceans require further investigation with regionally specific climatic forcing patterns.

Acknowledgments

The main part of this study is carried out during the first author's Ph.D. study at Georgia Institute of Technology. We thank Hartmut Frenzel for his technical support with the data processing of the CMIP5 archive and comments on the manuscript. We would also like to thank two anonymous reviewers for critical and constructive comments on the initial version of the manuscript. We acknowledge the World Climate Research Programme's Working Group on Coupled Modeling, which is responsible for CMIP5, and we thank the climate modeling groups (listed in Table 1) for producing and making available their model output. For CMIP5 the U.S. Department of Energy's Program for Climate Model Diagnosis and Intercomparison provides coordinating support and led development of software infrastructure in partnership with the Global Organization for Earth System Science Portals. Some figures are visualized using the NCAR Command Language (NCL). The model output from the sensitivity experiments used in this study could be accessed from the Georgia Tech website (http://shadow.eas.gatech.edu/~Ito/webdata/data.html). YT's Ph.D. study and TI were supported by a grant from NSF (OCE-1357373) and CD was supported by grants from NSF (OCE-1458967 and OCE-1419323) and the Gordon and Betty Moore Foundation (GBMF #3775). YT's work at the Max Planck Institute for Meteorology are supported by the European Union's Horizon 2020 research and innovation programme under grant agreement No 641816 (CRESCENDO).

References

Bopp, L., Resplandy, L., Orr, J. C., Doney, S. C., Dunne, J. P., Gehlen, M., et al. (2013). Multiple stressors of ocean ecosystems in the 21st century: Projections with CMIP5 models. *Biogeosciences*, *10*(10), 6225–6245. https://doi.org/10.5194/bg-10-6225-2013

Bopp, L., et al. (2017). Ocean (de) oxygenation from the Last Glacial Maximum to the twenty-first century: Insights from Earth system models. *Philosophical Transactions of the Royal Society A*, *375*(2102). https://doi.org/10.1098/rsta.2016.0323

Bryan, K., & Lewis, L. J. (1979). A water mass model of the world ocean. *Journal of Geophysical Research*, *84*(C5), 2503–2517. https://doi.org/10.1029/JC084iC05p02503

Cabré, A., Marinov, I., Bernardello, R., & Bianchi, D. (2015). Oxygen minimum zones in the tropical Pacific across CMIP5 models: Mean state differences and climate change trends. *Biogeosciences*, *12*(18), 5429–5454. https://doi.org/10.5194/bg-12-5429-2015

Capotondi, A., Alexander, M. A., Bond, N. A., Curchitser, E. N., & Scott, J. D. (2012). Enhanced upper ocean stratification with climate change in the CMIP3 models. *Journal of Geophysical Research*, *117*, C04031. https://doi.org/10.1029/2011JC007409

Cocco, V., Joos, F., Steinacher, M., Frölicher, T. L., Bopp, L., Dunne, J., et al. (2013). Oxygen and indicators of stress for marine life in multi-model global warming projections. *Biogeosciences*, *10*(3), 1849–1868. https://doi.org/10.5194/bg-10-1849-2013

Codispoti, L. A. (1995). Biogeochemical cycles - Is the ocean losing nitrate? *Nature*, *376*(6543), 724–724. https://doi.org/10.1038/376724a0

Codispoti, L. A., Brandes, J. A., Christensen, J. P., Devol, A. H., Naqvi, S. W. A., Paerl, H. W., & Yoshinari, T. (2001). The oceanic fixed nitrogen and nitrous oxide budgets: Moving targets as we enter the anthropocene? *Scientia Marina*, *65*(S2), 85–105. https://doi.org/10.3989/scimar.2001.65s285

Collins, M. R., et al. (2013). Long-term climate change: Projections, commitments and irreversibility. In T. F. Stocker, D. Qin, G.-K. Plattner, M. Tignor, S. K. Allen, J. Boschung, et al. (Eds.), *Climate change 2013: The physical science basis. Contribution of Working Group I to the Fifth Assessment Report of the Intergovernmental Panel on Climate Change*, (pp. 1029–1136). Cambridge, United Kingdom and New York, NY, USA: Cambridge University Press. doi:https://doi.org/10.1017/CBO9781107415324.024

Collins, W. J., Bellouin, N., Doutriaux-Boucher, M., Gedney, N., Halloran, P., Hinton, T., et al. (2011). Development and evaluation of an Earth-System model – HadGEM2. *Geoscientific Model Development*, *4*(4), 1051–1075. https://doi.org/10.5194/gmd-4-1051-2011

Czeschel, R., Stramma, L., & Johnson, G. C. (2012). Oxygen decreases and variability in the eastern equatorial Pacific. *Journal of Geophysical Research*, *117*, C11019. https://doi.org/10.1029/2012JC008043

de Lavergne, C., Palter, J. B., Galbraith, E. D., Bernardello, R., & Marinov, I. (2014). Cessation of deep convection in the open Southern Ocean under anthropogenic climate change. *Nature Climate Change*, *4*(4), 278–282. https://doi.org/10.1038/nclimate2132

Deutsch, C., Berelson, W., Thunell, R., Weber, T., Tems, C., McManus, J., et al. (2014). Centennial changes in North Pacific anoxia linked to tropical trade winds. *Science*, *345*(6197), 665–668. https://doi.org/10.1126/science.1252332

Deutsch, C., Brix, H., Ito, T., Frenzel, H., & Thompson, L. (2011). Climate-forced variability of ocean hypoxia. *Science*, *333*(6040), 336–339. https://doi.org/10.1126/science.1202422

Deutsch, C., Emerson, S., & Thompson, L. (2006). Physical - biological interactions in North Pacific oxygen variability. *Journal of Geophysical Research*, *111*, C09S90. https://doi.org/10.1029/2005JC003179

Deutsch, C., Ferrel, A., Seibel, B., Pörtner, H. O., & Huey, R. B. (2015). Climate change tightens a metabolic constraint on marine habitats. *Science*, *348*(6239), 1132–1135. https://doi.org/10.1126/science.aaa1605

DeVries, T., & Deutsch, C. (2014). Large-scale variations in the stoichiometry of marine organic matter respiration. *Nature Geoscience*, *7*(12), 890–894. https://doi.org/10.1038/ngeo2300

Dufresne, J. L., Foujols, M. A., Denvil, S., Caubel, A., Marti, O., Aumont, O., et al. (2013). Climate change projections using the IPSL-CM5 Earth system model: From CMIP3 to CMIP5. *Climate Dynamics*, *40*(9-10), 2123–2165. https://doi.org/10.1007/s00382-012-1636-1

Dunne, J. P., John, J. G., Shevliakova, E., Stouffer, R. J., Krasting, J. P., Malyshev, S. L., et al. (2012). GFDL's ESM 2 global coupled climate–Carbon Earth system models. Part II: Carbon system formulation and baseline simulation characteristics. *Journal of Climate*, *26*(7), 2247–2267. https://doi.org/10.1175/JCLI-D-12-00150.1

Duteil, O., & Oschlies, A. (2011). Sensitivity of simulated extent and future evolution of marine suboxia to mixing intensity. *Geophysical Research Letters*, *38*, L06607. https://doi.org/10.1029/2011GL046877

Dutkiewicz, S., Sokolov, A. P., Scott, J., & Stone, P. H. (2005). A three-dimensional ocean-seaice-carbon cycle model and its coupling to a two-dimensional atmospheric model: Uses in climate change studies, Report 122, Joint Program of the Science and Policy of Global Change, M.I.T., Cambridge, Massatusetts.

Garcia, H. E., Locarnini, R. A., Boyer, T. P., Antonov, J. I., Baranova, O. K., Zweng, M. M., & Johnson, D. R. (2010). In S. Levitus (Ed.), *World Ocean Atlas 2009, Volume 3: Dissolved oxygen, apparent oxygen utilization, and oxygen saturation*, *NOAA Atlas NESDIS 70*, (p. 344). Washington, D.C.: U.S. Government Printing Office.

Gent, P. R., & McWilliams, J. C. (1990). Isopycnal mixing in ocean circulation models. *Journal of Physical Oceanography*, *20*(1), 150–155. https://doi.org/10.1175/1520-0485(1990)020<0150:IMIOCM>2.0.CO;2

Getzlaff, J., & Dietze, H. (2013). Effects of increased isopycnal diffusivity mimicking the unresolved equatorial intermediate current system in an Earth system climate model. *Geophysical Research Letters*, *40*, 2166–2170. https://doi.org/10.1002/grl.50419

Getzlaff, J., Dietze, H., & Oschlies, A. (2016). Simulated effects of southern hemispheric wind changes on the Pacific oxygen minimum zone. *Geophysical Research Letters*, *43*, 728–734. https://doi.org/10.1002/2015GL066841

Gillett, N. P., & Fyfe, J. C. (2013). Annular mode changes in the CMIP5 simulations. *Geophysical Research Letters*, *40*, 1189–1193. https://doi.org/10.1002/grl.50249

Giorgetta, M. A., Jungclaus, J., Reick, C. H., Legutke, S., Bader, J., Böttinger, M., et al. (2013). Climate and carbon cycle changes from 1850 to 2100 in MPI-ESM simulations for the Coupled Model Intercomparison Project phase 5. *Journal of Advances in Modeling Earth Systems*, *5*, 572–597. https://doi.org/10.1002/jame.20038

Gnanadesikan, A., Dunne, J. P., & John, J. (2012). Understanding why the volume of suboxic waters does not increase over centuries of global warming in an Earth system model. *Biogeosciences*, *9*(3), 1159–1172. https://doi.org/10.5194/bg-9-1159-2012

Gnanadesikan, A., Russell, J. L., & Zeng, F. (2007). How does ocean ventilation change under global warming? *Ocean Science*, *3*(1), 43–53. https://doi.org/10.5194/os-3-43-2007

Gruber, N. (2011). Warming up, turning sour, losing breath: Ocean biogeochemistry under global change. *Philosophical Transactions of the Royal Society A*, *369*(1943), 1980–1996. https://doi.org/10.1098/rsta.2011.0003

Held, I. M., & Soden, B. J. (2006). Robust responses of the hydrological cycle to global warming. *Journal of Climate*, *19*(21), 5686–5699. https://doi.org/10.1175/JCLI3990.1

Helm, K. P., Bindoff, N. L., & Church, J. A. (2011). Changes in the global hydrological-cycle inferred from ocean salinity. *Geophysical Research Letters*, *37*, L18701. https://doi.org/10.1029/2010GL044222

Ito, T., Bracco, A., Deutsch, C., Frenzel, H., Long, M., & Takano, Y. (2015). Sustained growth of the Southern Ocean carbon storage in a warming climate. *Geophysical Research Letters*, *42*, 4516–4522. https://doi.org/10.1002/2015GL064320

Ito, T., & Deutsch, C. (2013). Variability of the oxygen minimum zone in the tropical North Pacific during the late twentieth century. *Global Biogeochemical Cycles*, *27*, 1119–1128. https://doi.org/10.1002/2013GB004567

Ito, T., Follows, M. J., & Boyle, E. A. (2004). Is AOU a good measure of respiration in the oceans? *Geophysical Research Letters*, *31*, L17305. https://doi.org/10.1029/2004GL020900

Ito, T., Minobe, S., Long, M. C., & Deutsch, C. (2017). Upper ocean O_2 trends: 1958–2015. *Geophysical Research Letters*, *44*, 4214–4223. https://doi.org/10.1002/2017GL073613

Jiang, S., Stone, P. H., & Malanotte-Rizzoli, P. (1999). An assessment of the geophysical fluid dynamics laboratory ocean model with coarse resolution: Annual-mean climatology. *Journal of Geophysical Research*, *104*(C11), 25,623–25,645. https://doi.org/10.1029/1999jc900095

Kalnay, E., Kanamitsu, M., Kistler, R., Collins, W., Deaven, D., Gandin, L., et al. (1996). The NCEP/NCAR 40-year reanalysis project. *Bulletin of the American Meteorological Society*, *77*(3), 437–471. https://doi.org/10.1175/1520-0477(1996)077<0437:TNYRP>2.0.CO;2

Karstensen, J., Stramma, L., & Visbeck, M. (2008). Oxygen minimum zones in the eastern tropical Atlantic and Pacific oceans. *Progress in Oceanography*, *77*(4), 331–350. https://doi.org/10.1016/j.pocean.2007.05.009

Keeling, R. F., & Garcia, H. E. (2002). The change in oceanic O_2 inventory associated with recent global warming. *Proceedings of the National Academy of Sciences*, *99*(12), 7848–7853. https://doi.org/10.1073/pnas.122154899

Keeling, R. F., Körtzinger, A., & Gruber, N. (2010). Ocean deoxygenation in a warming world. *Annual Review of Marine Science*, *2*(1), 199–229. https://doi.org/10.1146/annurev.marine.010908.163855

Large, W. G., Mcwilliams, J. C., & Doney, S. C. (1994). Oceanic vertical mixing - A review and a model with a nonlocal boundary-layer parameterization. *Reviews of Geophysics*, *32*, 363–403. https://doi.org/10.1029/94rg01872

Levitus, S., & Boyer, T. (1994). *World Ocean Atlas 1994*, (Vol. 4, p. 117). Washington, D.C.: Temperature. NOAA Atlas NESDIS 4, U.S. Gov. Printing Office.

Levitus, S., Burgett, R., & Boyer, T. (1994). *World Ocean Atlas 1994*, (Vol. 3, p. 99). Washington, D.C.: Salinity. NOAA Atlas NESDIS 3, U.S. Gov. Printing Office.

Long, M. C., Deutsch, C., & Ito, T. (2016). Finding forced trends in oceanic oxygen. *Global Biogeochemical Cycles*, *30*, 381–397. https://doi.org/10.1002/2015GB005310

Lovenduski, N. S., Fay, A. R., & McKinley, G. A. (2015). Observing multidecadal trends in Southern Ocean CO_2 uptake: What can we learn from an ocean model? *Global Biogeochemical Cycles*, *29*, 416–426. https://doi.org/10.1002/2014GB004933

Lovenduski, N. S., McKinley, G. A., Fay, A. R., Lindsay, K., & Long, M. C. (2016). Partitioning uncertainty in ocean carbon uptake projections: Internal variability, emission scenario, and model structure. *Global Biogeochemical Cycles*, *30*, 1276–1287. https://doi.org/10.1002/2016GB005426

Luyten, J. R., Pedlosky, J., & Stommel, H. (1983). The ventilated thermocline. *Journal of Physical Oceanography*, *13*(2), 292–309. https://doi.org/10.1175/1520-0485(1983)013<0292:TVT>2.0.CO;2

Ma, J., & Xie, S. P. (2013). Regional patterns of sea surface temperature change: A source of uncertainty in future projections of precipitation and atmospheric circulation. *Journal of Climate*, *26*(8), 2482–2501. https://doi.org/10.1175/JCLI-D-12-00283.1

Marshall, G. J. (2003). Trends in the southern annular mode from observations and reanalyses. *Journal of Climate*, *16*(24), 4134–4143. https://doi.org/10.1175/1520-0442(2003)016<4134:TITSAM>2.0.CO;2

Marshall, J., Adcroft, A., Hill, C., Perelman, L., & Heisey, C. (1997). A finite-volume, incompressible Navier Stokes model for studies of the ocean on parallel computers. *Journal of Geophysical Research*, *102*(C3), 5753–5766. https://doi.org/10.1029/96jc02775

Marshall, J., Hill, C., Perelman, L., & Adcroft, A. (1997). Hydrostatic, quasi-hydrostatic, and nonhydrostatic ocean modeling. *Journal of Geophysical Research*, *102*(C3), 5733–5752. https://doi.org/10.1029/96jc02776

Matear, R. J., & Hirst, A. C. (2003). Long-term changes in dissolved oxygen concentrations in the ocean caused by protracted global warming. *Global Biogeochemical Cycles*, *17*(4), 1125. https://doi.org/10.1029/2002GB001997

McKinley, G. A., Fay, A. R., Lovenduski, N., & Pilcher, D. J. (2017). Natural variability and anthropogenic trends in the ocean carbon sink. *Annual Review of Marine Science*, *9*(1), 125–150. https://doi.org/10.1146/annurev-marine-010816-060529

McKinley, G. A., Pilcher, D. J., Fay, A. R., Lindsay, K., Long, M. C., & Lovenduski, N. S. (2016). Timescales for detection of trends in the ocean carbon sink. *Nature*, *530*(7591), 469–472. https://doi.org/10.1038/nature16958

Meinshausen, M., Smith, S. J., Calvin, K., Daniel, J. S., Kainuma, M. L. T., Lamarque, J. F., et al. (2011). The RCP greenhouse gas concentrations and their extension from 1765 to 2300. *Climatic Change*, *109*(1-2), 213–241. https://doi.org/10.1007/s10584-011-0156-z

Moore, J. K., Lindsay, K., Doney, S. C., Long, M. C., & Misumi, K. (2013). Marine ecosystem dynamics and biogeochemical cycling in the community Earth system model [CESM1(BGC)]: Comparison of the 1990s with the 2090s under the RCP4.5 and RCP8.5 scenarios. *Journal of Climate*, *26*(23), 9291–9312. https://doi.org/10.1175/JCLI-D-12-00566.1

Oschlies, A., Brandt, P., Stramma, L., & Schmidtko, S. (2018). Drivers and mechanisms of ocean deoxygenation. *Nature Geoscience*, *1*. https://doi.org/10.1038/s41561-018-0152-2

Oschlies, A., Shulz, K. G., Riebesell, U., & Schmittner, A. (2008). Simulated 21st century's increase in oceanic suboxia by CO_2-enhanced biotic carbon export. *Global Biogeochemical Cycles*, *22*, GB4008. https://doi.org/10.1029/2007GB003147

Parekh, P., Follows, M. J., & Boyle, E. A. (2005). Decoupling of iron and phosphate in the global ocean. *Global Biogeochemical Cycles*, *19*, GB2020. https://doi.org/10.1029/2004GB002280

Redi, M. H. (1982). Oceanic isopycnal mixing by coordinate rotation. *Journal of Physical Oceanography*, *12*(10), 1154–1158. https://doi.org/10.1175/1520-0485(1982)012<1154:OIMBCR>2.0.CO;2

Ridder, N., & England, M. H. (2014). Sensitivity of ocean oxygenation to variations in tropical zonal wind stress magnitude. *Global Biogeochemical Cycles*, *28*, 909–926. https://doi.org/10.1002/2013GB004708

Schmidtko, S., Stramma, L., & Visbeck, M. (2017). Decline in global oceanic oxygen content during the past five decades. *Nature*, *542*(7641), 335–339. https://doi.org/10.1038/nature21399

Schneider, T., O'Gorman, P. A., & Levine, X. J. (2010). Water vapor and the dynamics of climate changes. *Reviews of Geophysics*, *48*, RG3001. https://doi.org/10.1029/2009RG000302

Seibel, B. A. (2010). Critical oxygen levels and metabolic suppression in oceanic oxygen minimum zones. *The Journal of Experimental Biology*, *214*(2), 326–336. https://doi.org/10.1242/jeb.049171

Shigemitsu, M., Yamamoto, A., Oka, A., & Yamanaka, Y. (2017). One possible uncertainty in CMIP5 projections of low-oxygen water volume in the eastern tropical Pacific. *Global Biogeochemical Cycles*, *31*, 804–820. https://doi.org/10.1002/2016GB005447

Solomon, A., & Polvani, L. M. (2016). Highly significant responses to anthropogenic forcings of the midlatitude jet in the southern hemisphere. *Journal of Climate*, *29*(9), 3463–3470. https://doi.org/10.1175/JCLI-D-16-0034.1

Stramma, L., Johnson, G. C., Firing, E., & Schmidtko, S. (2010). Eastern Pacific oxygen minimum zones: Supply paths and multidecadal changes. *Journal of Geophysical Research*, *115*, C09011. https://doi.org/10.1029/2009JC005976

Stramma, L., Johnson, G. C., Sprintall, J., & Mohrholz, V. (2008). Expanding oxygen-minimum zones in the tropical oceans. *Science*, *320*(5876), 655–658. https://doi.org/10.1126/science.1153847

Stramma, L., Oschlies, A., & Schmidtko, S. (2012). Mismatch between observed and modeled trends in dissolved upper-ocean oxygen over the last 50 yr. *Biogeosciences*, *9*(10), 4045–4057. https://doi.org/10.5194/bg-9-4045-2012

Swart, N. C., Fyfe, J. C., Gillett, N., & Marshall, G. J. (2015). Comparing trends in the southern annular mode and surface westerly jet. *Journal of Climate*, *28*(22), 8840–8859. https://doi.org/10.1175/JCLI-D-15-0334.1

Taylor, K. E., Stouffer, R. J., & Meehl, G. A. (2012). An overview of CMIP5 and the experiment design. *Bulletin of the American Meteorological Society*, *93*(4), 485–498. https://doi.org/10.1175/BAMS-D-11-00094.1

The NCAR Command Language (Version 6.3.0) [Software] (2016). Boulder, Colorado: UCAR/NCAR/CISL/TDD. https://doi.org/10.5065/D6WD3XH5

Thomas, R. K., Fanrong, Z., & Andrew, T. W. (2013). Multimodel assessment of regional surface temperature trends: CMIP3 and CMIP5 twentieth-century simulations. *Journal of Climate*, *26*(22), 8709–8743. https://doi.org/10.1175/JCLI-D-12-00567.1

Thompson, D. W., Wallace, J. M., & Hegerl, G. C. (2000). Annular modes in the extratropical circulation, Part II: Trends. *Journal of Climate*, *13*(5), 1018–1036. https://doi.org/10.1175/1520-0442(2000)013<1018:AMITEC>2.0.CO;2

Tokinaga, H., Xie, S. P., Deser, C., Kosaka, Y., & Okumura, Y. M. (2012). Slowdown of the Walker circulation driven by tropical Indo-Pacific warming. *Nature*, *491*(7424), 439–443. https://doi.org/10.1038/nature11576

Trenberth, K., Olson, J., & Large, W., (1989). A global wind stress climatology based on ECMWF analyses, *Tech. Rep. NCAR/TN-338+STR*, National Center for Atmospheric Research, boulder, Colorado.

Vallis, G. K., Zurita-Gotor, P., Cairns, C., & Kidston, J. (2015). Response of the large-scale structure of the atmosphere to global warming. *Quarterly Journal of the Royal Meteorological Society*, *141*(690), 1479–1501. https://doi.org/10.1002/qj.2456

Vaquer-Sunyer, R., & Duarte, C. M. (2008). Thresholds of hypoxia for marine biodiversity. *Proceedings of the National Academy of Sciences*, *105*(40), 15,452–15,457. https://doi.org/10.1073/pnas.0803833105

Vecchi, G. A., Soden, B. J., Wittenberg, A. T., Held, I. M., Leetmaa, A., & Harrison, M. J. (2006). Weakening of tropical Pacific atmospheric circulation due to anthropogenic forcing. *Nature*, *441*(7089), 73–76. https://doi.org/10.1038/nature04744

Voss, M., Bange, H. W., Dippner, J. W., Middelburg, J. J., Montoya, J. P., & Ward, B. (2013). The marine nitrogen cycle: Recent discoveries, uncertainties and the potential relevance of climate change. *Philosophical Transactions of the Royal Society, B: Biological Sciences*, *368*(1621). 20130121. https://doi.org/10.1098/rstb.2013.0121

Weber, T., Cram, J. A., Leung, S. W., DeVries, T., & Deutsch, C. (2016). Deep ocean nutrients imply large latitudinal variation in particle transfer efficiency. *Proceedings of the National Academy of Sciences*, *113*(31), 8606–8611. https://doi.org/10.1073/pnas.1604414113

Xie, S. P., Deser, C., Vecchi, G., Ma, J., Teng, H., & Wittterberg, A. (2010). Global warming pattern formation: Sea surface temperature and rainfall. *Journal of Climate*, *23*(4), 966–986. https://doi.org/10.1175/2009JCLI3329.1